Available online at www.sciencedirect.com

ScienceDirect

Underground Space 26 (2026) 126–151

www.keaipublishing.com/undsp

Research Paper

Thrust-vectoring automatic shield tunneling technology: Method, verification and application

Yeting Zhu [a], Di Wu [b], Zhihua Wang [a,c], Zixin Zhang [d], Shuaifeng Wang [d], Xin Huang [d,e,*], Yuan Qin [a], Yanfei Zhu [a], Fan Wang [c]

[a] *Shanghai Tunnel Engineering Co., Ltd., Shanghai 200232, China*
[b] *Shanghai Shentong Metro Co., Ltd., Shanghai 201102, China*
[c] *School of Civil Engineering and Hydraulic Engineering, Huazhong University of Science and Technology, Wuhan 430074, China*
[d] *Department of Geotechnical Engineering, Tongji University, Shanghai 200092, China*
[e] *College of Civil Engineering and Architecture, Xinjiang University, Urumqi 830046, China*

Received 27 October 2024; received in revised form 20 December 2024; accepted 20 January 2025
Available online 24 October 2025

Abstract

Recognizing the formidable challenge of achieving millimeter-level precision in controlling shield machine attitudes amidst thrust forces exceeding thousands of tons on a global scale, a thrust-vectoring automatic shield tunneling technology was introduced to effectively mitigate potential inaccuracies stemming from human intervention. Initially, a load-thrust "dual-vector" motion control mechanism was adopted, grounded in defining the shield thrust vector and establishing the interactive correlation between shield attitude deviation points and thrust action points in both horizontal and vertical orientations through comprehensive data assessments. Subsequently, a parallel proportional-integral-derivative control law was devised for stability control of shield machines, delineating the functional link between alterations in shield attitudes and displacements of thrust action points, with initial validation conducted via full-scale model trials. A motion trajectory for correcting shield attitudes was devised, and a thrust vector control approach was formulated by amalgamating feedforward calculations with feedback adjustments. The application of this thrust-vectoring automatic tunneling technology in a large-diameter shield tunneling endeavor yielded the subsequent key findings: a consistent deviation of approximately 2.5% was upheld between target and actual thrust forces, with actual shield velocity managed within a –1 to +1 mm/min range from the target value. To ensure robust steering capability of the shield machine, target thrust moments in both horizontal and vertical directions marginally exceeded actual values, with satisfactory execution. The interplay between shield attitudes and thrust action points in both horizontal and vertical dimensions exhibited a characteristic akin to "sugar-coated haws on a stick". Despite notable "kowtow" occurrences during segment assembly, statistical analysis indicated that deviations in shield attitude in horizontal and vertical planes were ultimately contained within –20 to +5 mm and –45 to –28 mm ranges, respectively, markedly surpassing average manual control standards.

Keywords: Shield machine; Automatic shield tunneling; Shield attitude; Thrust vector; Control law; Model test platform; Engineering application

1 Introduction

The shield tunneling method has become the predominant technique for constructing long urban tunnels in soft, composite, and even rock strata due to its high efficiency and safety (Qian et al., 2024). As one of the most mechanized processes in civil engineering, many fundamental automatic control challenges within shield machines were addressed as early as the 1980s. These advancements included the regulation of chamber soil pressure, synchronous grouting, cutterhead rotation speed, and penetration depth. Despite these developments, the precise control of shield machine attitudes

* Corresponding author at: Department of Geotechnical Engineering, Tongji University, Shanghai 200092, China.
E-mail address: xhuang@tongji.edu.cn (X. Huang).
Peer review under the responsibility of Tongji University

https://doi.org/10.1016/j.undsp.2025.01.008

remains heavily reliant on manual operation experience (Zheng et al., 2024).

During shield advancement along the designed tunnel axis (DTA), operators must closely monitor the shield attitudes as indicated by the guidance system and manually control the thrust distribution of the propulsion system, which consists of dozens of hydraulic cylinders. To simplify this process, the cylinders are typically grouped into four or six fixed units (Wang et al., 2022), i.e., the cylinders within each group share a common oil pressure. Operators then adjust the target oil pressure of each propulsion group based on their experience to ensure that the shield machine's movement trajectory fits complex boundary conditions, such as maintaining shield attitude deviations within allowable thresholds, minimizing surface settlement caused by excessive formation loss (Tian & Wang, 2023), and ensuring uniform circumferential clearance at the shield tail to facilitate the assembly of tunnel segments (Zeng et al., 2022).

In recent decades, the scale of shield tunnel construction has continued to expand rapidly and is expected to maintain a high growth trend in the future. This, however, is not compatible with the dilution of a well-trained workforce, shrinking working-age population, and rising labor costs. As the complexity of shield tunnel projects increases and construction timelines continue to shorten, the traditional reliance on oral transmission of operational experience between masters and apprentices is becoming increasingly unsustainable. This reliance leads to significant fluctuations in construction quality and increases the risk of safety incidents, imposing unpredictable difficulties and costs on the future operation and maintenance of completed tunnels. Given these challenges, the adoption of intelligent methods to achieve automatic shield tunneling manifests itself as the optimal solution for eliminating the need for human intervention.

Currently, studies on the attitude control of shield machines primarily focus on theoretical analysis, predictive modeling, and intelligent control. In terms of theoretical analysis, typical findings include: Yue et al. (2012) analyzed the dynamics of the shield postures to describe the coupling effect of the equivalent loads and actuators; Festa et al. (2015) quantified the radial soil displacements induced by a shield machine driving in soft strata; Wang et al. (2018) proposed a mathematical method for determining the target motions of thrust cylinders to control the shield pose; Liu et al. (2019) proposed a novel rectification trajectory planning method for TBM according to the different attitude deviations and target path; Tang et al. (2022) developed a calculation model of posture rectification load of an earth pressure balance shield. The existing research achievements in predictive modeling primarily leverage machine learning methods, including the extreme gradient boosting model (Wang et al., 2019), gated recurrent unit (GRU) model (Li et al., 2020), adaptive neuro-fuzzy inference system model (He et al., 2020), principal component analysis (PCA)-GRU model (Zhang et al., 2022), graph convolutional network-long and short-term memory (GCN-LSTM) model (Fu et al., 2023), and Convolutional-GRU model (Wang et al., 2023). These approaches have significantly enhanced the accuracy of shield attitude predictions. Methods for the automatic control of shield attitudes are primarily categorized into two approaches: traditional proportional-integral-derivative (PID) control methods (Jian et al., 2023; Ren et al., 2019; Zhang et al., 2023) and machine learning techniques (Cai, 2022; Fu et al., 2024; Hu et al., 2022; Jia et al., 2023; Xu et al., 2024; Zhang et al., 2022). However, aside from the intelligent system developed in Hu et al. (2022), which has been validated through multiple engineering projects and long-distance applications, other methods remain in the stages of experimental validation and technical optimization.

The aforementioned studies have significantly contributed to the advancement of automatic shield attitude control technology. However, three critical issues remain inadequately addressed. First, there is a lack of a rigorous scientific understanding of the motion control mechanism of shield machines, which forms the cornerstone of automatic shield tunneling technology. Although some achievements based on machine learning methods have been successfully applied in engineering, their limited interpretability becomes evident when facing abnormal situations. Second, the universality of existing technologies remains weak. Current machine learning approaches are highly dependent on high-quality data from specific engineering projects. When the shield machine equipment, geological conditions, or control requirements change, these technologies often require substantial optimization and adaptation to accommodate varying boundary conditions. Third, existing technologies exhibit poor generalizability across different shield equipment. This implies that they are either unsuitable for use with current equipment, requiring extensive modifications for newly manufactured machines, or lack interoperability with equipment from different manufacturers.

Additionally, a number of studies have been conducted on the computational methods for determining shield machine thrust and associated load forces. More specifically, Zhang et al. (2014) established a predicting model for the total load acting on the cutterhead that fully reflects the influences of geological, operating, and structural parameters; Sun et al. (2018) presented a dynamic load prediction approach based on heterogeneous in-situ data and a data-driven technique; Li and Gong (2019) established a model predictive control system for the slurry pressure; Kong et al. (2022) developed a load prediction approach of an earth pressure balance shield machine based on random forest machine learning method; Zhang et al. (2023) proposed an intelligent real-time prediction method for multi-region thrust of EPB shield machine based on a sparrow search algorithm-long and short-term memory model; Wang et al. (2023) established a thrust prediction model for the TBM based on the combination of on-site quality

record data and surrogate model technology; Soranzo et al. (2023) proposed the deep Q-network algorithm to predict the face support pressure; Xie et al. (2024) developed a building information modeling (BIM)-based multi-model framework to achieve an automated workflow from BIM-based multi-model of shield tunneling to real-time thrust calculations.

The aforementioned literature has primarily focused on the calculation and prediction of thrust force, which has significantly contributed to the design of shield machine propulsion systems, face stability control, and shield machine start-up processes. However, due to insufficient consideration of attitude control, these outcomes cannot be directly applied to the automatic control systems required for shield tunneling operations.

In this study, a novel thrust-vectoring technology was introduced to the field of shield tunneling for the first time, with the aim of moving beyond traditional trend-based control of shield attitudes and developing a precise thrust vector control method to enable automatic operation of shield machines. After uncovering the motion control mechanism of the shield machine, a parallel PID control law for shield attitude regulation was formulated to establish the relationship between changes in shield attitudes and the displacement of thrust action points. Subsequently, motion path planning and navigation technology based on manual operation experience was developed, and an automatic thrust-vectoring control system was implemented to achieve precise execution of target steering angles in both the horizontal and vertical directions. The feasibility, reliability, and interpretability of this technology were thoroughly validated through full-scale model testing and its practical application in a large-diameter shield tunneling project.

2 Correlation between shield attitudes and thrust vector

2.1 Balance control principle for both shield cutterhead and tail

When a shield machine advances through soft soil or composite strata, its attitudes are primarily influenced by three key factors: pressure balance in the cutterhead, slurry grouting at the shield tail, and thrust control within the propulsion system. Of these, the first two are also crucial components of surface subsidence management.

As illustrated in Fig. 1, effective pressure management in the cutterhead involves two primary types of balance: material balance and pressure balance. Material balance aims to ensure an equal volume exchange between soil excavation and spoil removal, while pressure balance is designed to effectively support the tunnel face, prevent instability, and minimize disturbances to the surrounding ground. From an automatic control perspective, once the target advancement speed of the shield machine is set, the pressure within the slurry chamber (or earth pressure chamber) can be regulated by correlating it with the flow rate difference between slurry supply and discharge (or the rotation speed of the screw conveyor) through a closed-loop control system, thereby enabling automatic adjustment.

The primary objective of synchronous grouting at the shield tail is to maintain material balance, specifically to provide volumetric compensation for ground loss. The total slurry volume required for a single segmental ring is initially calculated using theoretical formulas and then dynamically adjusted based on the observed surface settlement behavior in the current ring being excavated by the shield machine. Subsequently, a proportionate volume of slurry, determined in accordance with the total dosage, is automatically grouted in synchronization with the net stroke of the propulsion system. In addition to the grouting operation, the properties of the slurry itself are important due to the influence on the uplift performance of both the shield tail and the segments. Both engineering practice and in-situ testing have demonstrated that dual-component slurries offer significant advantages over single-component slurries (Huai et al., 2022).

It is noteworthy that automatic control of pressure balance in the shield cutterhead, as well as synchronous grouting at the shield tail, has been successfully implemented since the 1980s. In recent years, researchers (Hu et al., 2022) have further enhanced the control performance of these systems by incorporating machine learning techniques. Consequently, this paper shifts the focus toward the active control of thrust vector in the propulsion system, with the aim of optimizing shield machine maneuverability and stability.

2.2 Definition of shield thrust vector

The definition of the shield thrust vector $\boldsymbol{F}_{\mathrm{T}}$ is depicted in Fig. 2. In reference to the shield tunneling direction, the center of the propulsion system is designated as the origin o, the rightward direction along the horizontal symmetry axis and the upward direction along the vertical symmetry axis are defined as the positive directions of the x-axis and y-axis, respectively. The z-axis is perpendicular to the xoy plane, with the positive direction pointing toward the cutterhead. The distances from each propulsion force generated by the corresponding hydraulic cylinder (F_i, $i = 1$–n) to the x- and y-axes are defined as the force arms (e_x and e_y), with the direction consistent with the positive z-axis. Based on these definitions, the thrust force $\| \boldsymbol{F}_{\mathrm{T}} \|$, along with its horizontal and vertical moments (M_{Th} and M_{Tv}), can be calculated, as well as the coordinates of the shield thrust action point S_0 (S_x,S_y).

$$\| \boldsymbol{F}_{\mathrm{T}} \| = \sum_{i=1}^{n} F_i, \tag{1}$$

$$(S_x, S_y) = \left(\frac{\sum_{i=1}^{n} F_i e_{xi}}{\sum_{i=1}^{n} F_i}, \frac{\sum_{i=1}^{n} F_i e_{yi}}{\sum_{i=1}^{n} F_i} \right), \tag{2}$$

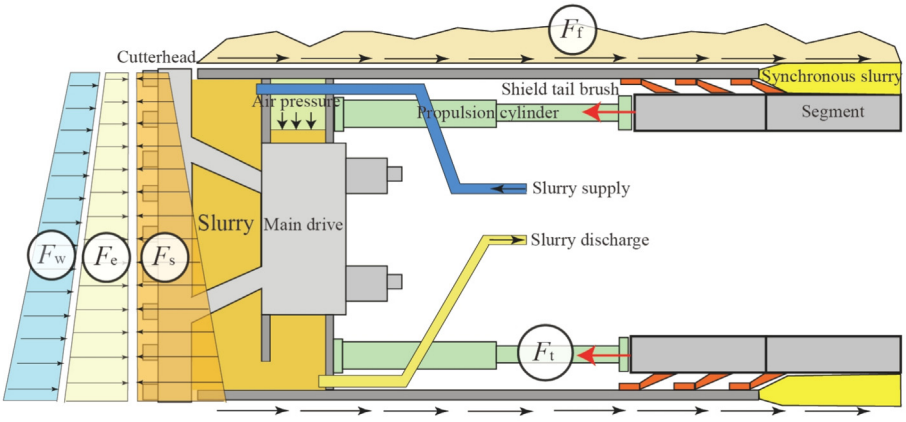

Fig. 1. Working principle of shield tunneling (F_w and F_e are the static water and earth pressures at the tunneling face, F_s is the support force generated from the slurry chamber, F_f is the shield shell skin friction, and F_t is the thrust generated by the propulsion cylinder).

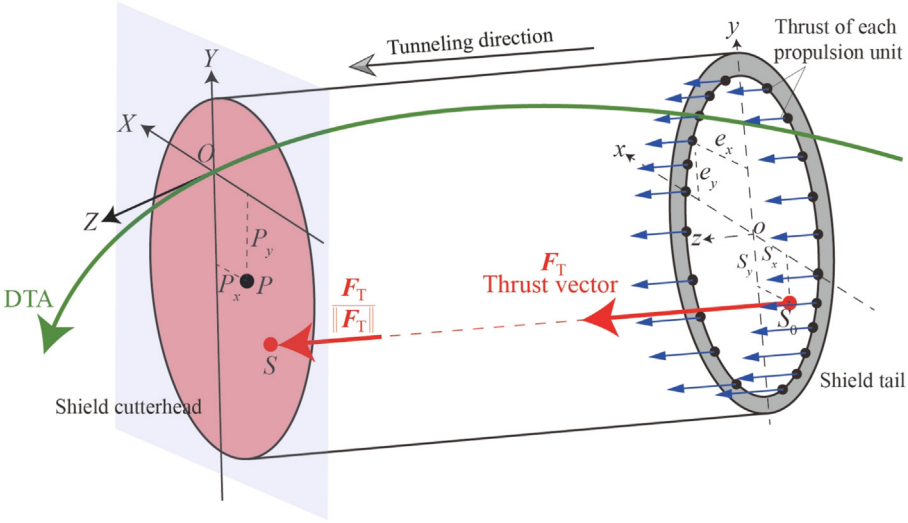

Fig. 2. Schematic diagram of shield thrust vector.

$$(M_{Th}, M_{Tv}) = \left(\| \boldsymbol{F}_T \| S_x, \| \boldsymbol{F}_T \| S_y\right), \tag{3}$$

where n stands for the number of the propulsion cylinder units.

Subsequently, a three-dimensional angular coordinate system is established, with the intersection point between the vertical plane containing the shield cutterhead's attitude measurement point and the DTA as the origin O (see Fig. 2). The rightward direction along the horizontal axis and the upward direction along the vertical axis are defined as the positive directions of the X- and Y-axes, respectively. The Z-axis is perpendicular to the XOY plane, with its positive direction aligned with the tunneling direction. In this coordinate system, both the attitude deviation points of the shield cutterhead $P(P_x,P_y)$ and the projection of the action point S of the shield thrust vector lie within the XOY plane.

In fact, the shield attitude deviations are within the centimeter range, which is negligible compared to the size of the shield machine. Similarly, the dimensions of the shield machine can also be considered insignificant in relation to the tunnel axis. Therefore, it can be reasonably assumed that the Z-axis coincides with both the tangent to the DTA and the direction of the shield thrust vector, the positive directions of the three axes in the O-XYZ coordinate system can be considered consistent with those in the o-xyz coordinate system. The unit vector of the shield thrust in the three-dimensional coordinate system is expressed as its direction components $(S_x, S_y, 1)$. Ultimately, the shield thrust vector is defined as follows:

$$\boldsymbol{F}_T = \| \boldsymbol{F}_T \| (S_x, S_y, 1). \tag{4}$$

Finally, the coordinates for P and S can be directly utilized in the following analysis.

2.3 Engineering case study

2.3.1 Data sources

We conducted an extensive investigation into the spatial interaction between the shield thrust action point and the shield attitude deviation point in three representative shield

tunneling projects, Shanghai Airport Railway Link Line, Nanjing Jianning West Road Yangtze River Tunnel, and Shenzhen Mawan Cross-Sea Tunnel, operated under manual control, corresponding to soft, composite, and rock strata, respectively.

(1) The Shanghai Airport Railway Link Line is an urban rapid transit system running along the east–west axis of Shanghai, connecting Pudong International Airport and Hongqiao International Airport. A key section of this project, spanning 2170 m from the working shaft at Meifu Road to the reception shaft at Huajing Station, was constructed using a mixed-mode shield machine with a super-large diameter of 14.07 m. This geological section mainly consists of silty clay and silty sand interbedded with silty clay. The variations in the coordinates of the shield thrust action point, along with the corresponding attitude deviations of the shield cutterhead in both the horizontal and vertical directions, were recorded for rings 701–855 (a total of 155 rings) in the soft strata, as presented in Fig. 3.

(2) The Nanjing Jianning West Road Yangtze River Tunnel extends from Hengjiang Avenue on the north bank of the river to Huimin Road on the south bank, in China. The shield tunnel in Lot 2 of this project, with a total length of 2.361 km, crosses typical composite strata characterized by soft upper layers and hard lower layers. The upper layer consists of loose fine sand, while the lower layer is composed of round gravel interbedded with pebbles. This section was excavated using a super-large slurry balance shield machine with a diameter of 15.07 m. The variations in the coordinates of the shield thrust action point and the corresponding attitude deviations of the shield cutterhead, in both horizontal and vertical directions, were monitored for rings 349–431 (a total of 83 rings), as presented in Fig. 4.

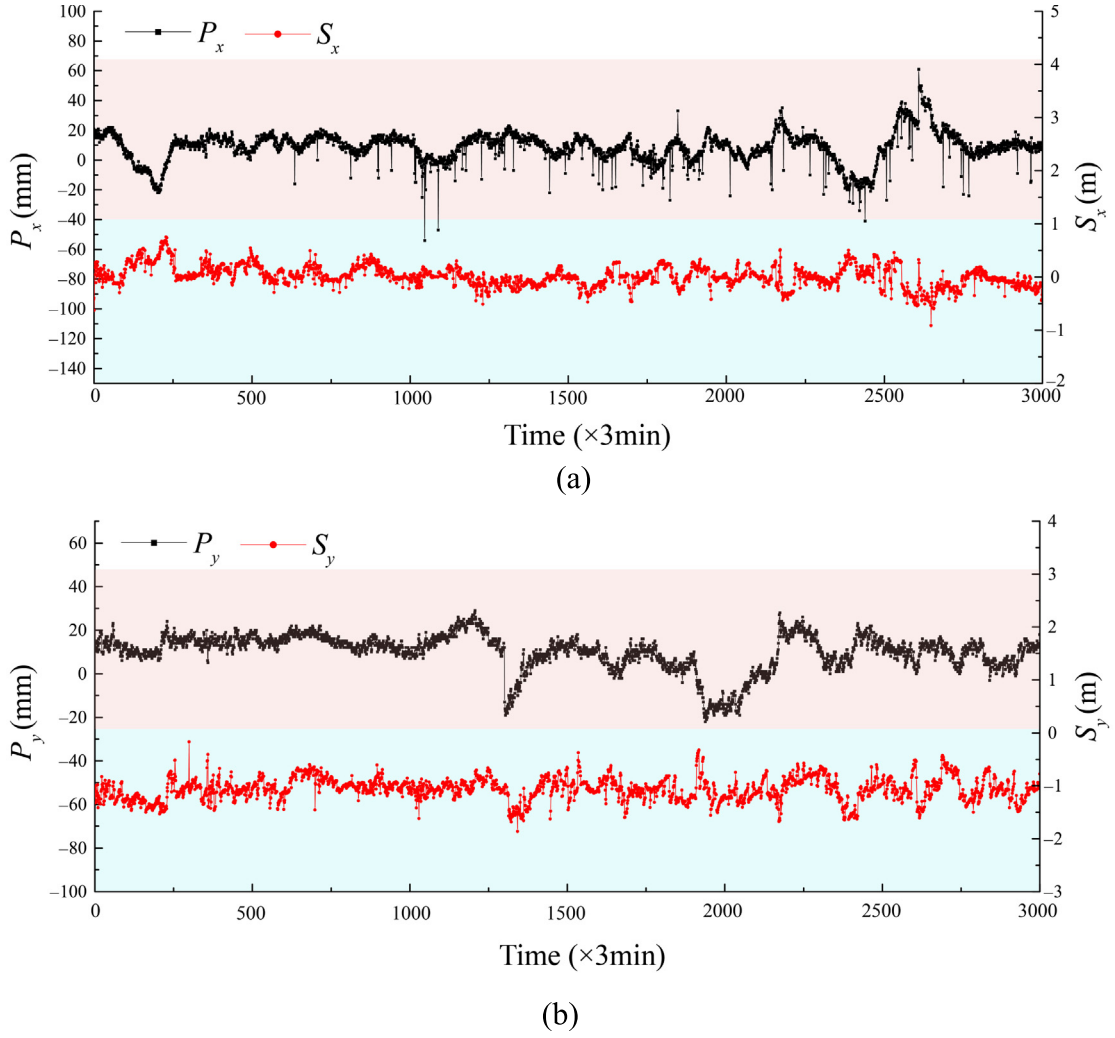

Fig. 3. Variations of the coordinates of the shield thrust action point and the attitude deviations of the shield cutterhead with time in soft strata. (a) Horizontal direction, and (b) vertical direction.

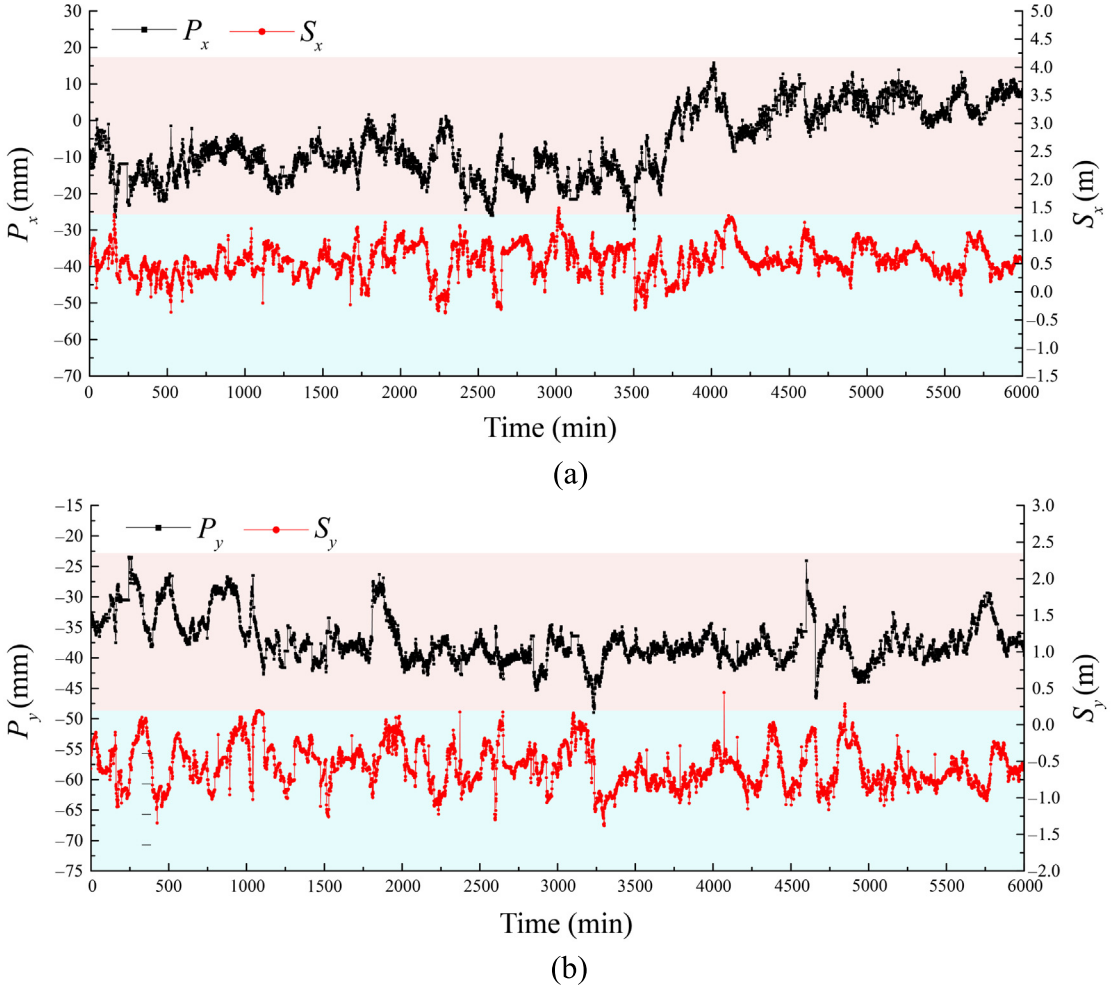

Fig. 4. Variations of the coordinates of the shield thrust action point and the attitude deviations of the shield cutterhead with time in composite strata. (a) Horizontal direction, and (b) vertical direction.

(3) The Shenzhen Mawan Cross-Sea Tunnel begins at the intersection of Mawan Avenue and Moon Bay Avenue and terminates at the intersection of Jinwan Avenue and Xixiang Avenue in China. This tunnel spans a total length of 2060 m and was excavated using a mixed-mode shield machine of a super-large diameter 15.55 m. Hard rock strata account for 37.5% of the entire tunnel alignment, with significant variability in rock strength throughout this section. The average uniaxial compressive strength of the rock is 65 MPa, with a maximum value reaching 169.8 MPa. The variations in the coordinates of the shield thrust action point, along with the corresponding attitude deviations of the shield cutterhead in both horizontal and vertical directions, were recorded for rings 573–616 (a total of 44 rings) in the rock strata (Fig. 5).

2.3.2 Data analysis

As illustrated in Figs. 3–5, the coordinates of the thrust action point and the attitude deviations of the shield cutterhead exhibit a discernible spatial interaction. This interaction is characterized by an inverse relationship, where movement of the thrust action point in one direction is accompanied by a corresponding shift in the shield cutterhead's attitude in the opposite direction. This "forward–backward" dynamic is reflected in the mirror symmetry observed between the variation curves of both parameters, which display a high degree of correlation when plotted on the same graph.

In practical tunneling operations, due to the relatively stable nature of the load vector over short time intervals or distances, shield operators can steer the machine toward the target direction by adjusting the distribution of thrust forces across the various propulsion zones, based on their experience. Fundamentally, the operators' actions involve dynamically adjusting the position of the shield thrust action point (S_x,S_y) to ensure that the changing of the thrust force moments meets the steering requirements.

Once the position of the thrust action point is adjusted, the attitude deviations of the shield cutterhead will undergo a corresponding change, which finally results in the mirror symmetry feature as demonstrated in Figs. 3–5. Therefore, there must be quantifiable functional relationships to

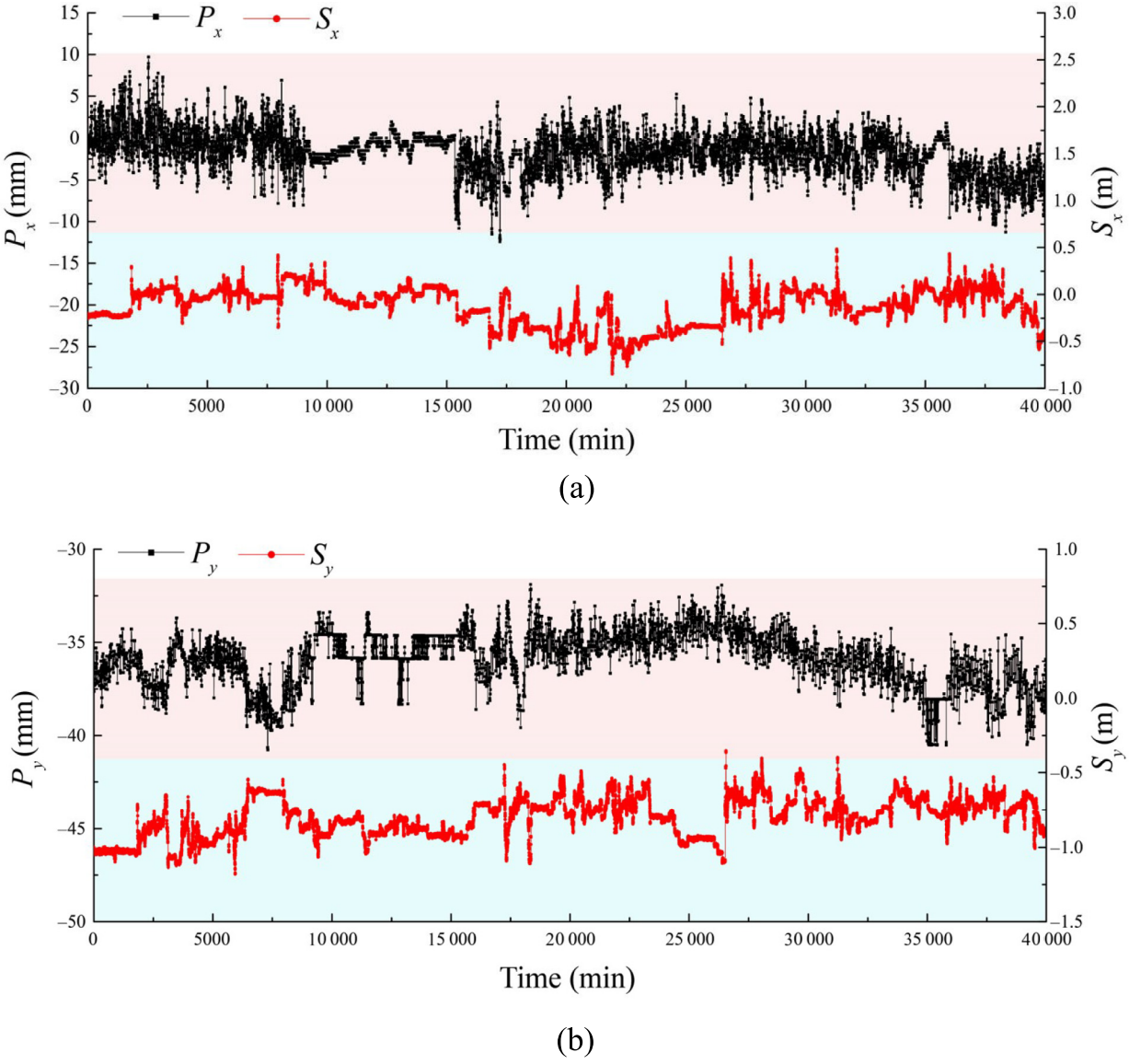

Fig. 5. Variations of the coordinates of the shield thrust action point and the attitude deviations of the shield cutterhead with time in rock strata. (a) Horizontal direction, and (b) vertical direction.

express the correlation between the changes in the shield attitudes $\Delta P_{x,y}$ and the location of the thrust action point $\Delta S_{x,y}$, which can be articulated as Eq. (2). Furthermore, this functional relationship lays the foundation for adopting the thrust-vectoring technology to achieve automatic control of the shield attitudes in this paper.

$$\Delta S_{x,y} = f\left(\Delta P_{x,y}\right) \tag{5}$$

It is worth noting that the shield attitudes may exhibit a slight delay relative to the movement of the thrust action point. Given that the shield machine's burial depth remains relatively consistent in the horizontal direction, while its attitude in the vertical direction is influenced by multiple factors, such as the mass distribution of the shield machine, variations in burial depth, and the cutting efficiency of the upper and lower soil layers, the shield attitude response is more sensitive in the horizontal direction compared to the vertical direction. Both the data analysis and practical operational feedback suggest that adjusting the shield attitude in the vertical direction is more challenging than in the horizontal direction.

An intriguing phenomenon was then observed: as the stiffness of the strata increases from soft ground to rock formations, the frequency of shield attitude fluctuations intensifies. This increase may be attributed to the vibrations induced by the interaction between the cutting tools and the rock. Nevertheless, regardless of the geological conditions, the shield attitudes are primarily controlled through manual adjustments of the thrust vector in the propulsion system under the premise of ensuring the optimal cutting performance of the cutting tools.

3 Design of steady-state shield tunneling control law

The term "control law" (Zhen et al., 2024) originates from the field of aviation equipment and is an algorithm to form the flight control instructions, which can characterize the functional relationship between controlled state variables and system input signals. Based on the correlation between shield attitudes and thrust vectors presented in Section 2, this study applies the control law for the first time in the field of shield construction. We will first reveal the motion control mechanism of the shield machine in Section 3.1, then establish a dedicated control law to achieve the steady-state shield tunneling in Section 3.2, enabling the precise regulation of both the shield attitudes and shield speed. The system input signal corresponds to the desired variations in shield attitudes, while the controlled state variables are the thrust vectors. The target variations in shield attitudes will be defined through the motion path planning technique outlined in Section 3.2, and the control methodology for the thrust vector will be detailed in Section 3.4.

3.1 Motion control mechanism of shield machine

The structural stiffness of the shield machine is significantly higher than that of the surrounding strata. Hence, as illustrated in Fig. 6, the shield machine can be reasonably approximated as a rigid body enveloped by the surrounding geological materials. The interaction between the shield machine and the surrounding soil can be simplified using a soil spring model. Consequently, the loads acting on the shield machine in the vertical direction (including its self-weight, the earth pressure, etc.) can be balanced by the reaction force from the soil springs. Furthermore, the water and soil pressures acting on the cutterhead, the lateral frictional resistance on the shell, and the different cutting efficiency of the cutters in different soil layers can all be classified as load vector $\boldsymbol{F}_{\mathrm{L}}$ in the direction of shield tunneling. Based on the research and development team's years of construction experience, when the shield tunnels over relatively short distances or durations, the changes in load vector are minimal, thus allowing sufficient adjustment time for active control of the thrust vector.

Finally, the kinematic model of the shield machine advancing at a constant speed can be simplified into a "dual vector" model (see Fig. 6), comprising the load vector and the thrust vector. These two vectors, of equal magnitude, form a force couple. By considering the distance d_{couple} between the two vectors, the moment vector of the force couple $\boldsymbol{M}_{\mathrm{shield}}$ can be expressed as

$$\boldsymbol{M}_{\mathrm{shield}} = \boldsymbol{F}_{\mathrm{T}} d_{\mathrm{couple}}, \tag{6}$$

where $\boldsymbol{F}_{\mathrm{T}}$ is the thrust vector.

The moment vector of the force couple possesses both direction and magnitude. The direction dictates the yaw orientation of the shield machine, and the magnitude governs the yaw rate.

By aligning the two coordinate systems shown in Fig. 2, a clear correspondence can be identified between the displacements of the thrust action point (ΔS_x and ΔS_y) and the variations in shield attitude (ΔP_x and ΔP_y), as depicted in Fig. 7. The primary objective of this study is to investigate this interaction to facilitate the automatic control of shield machine attitude.

3.2 Establishment of parallel PID control system

Among the various control strategies, the PID control law is widely regarded as the most robust. Its key advantage lies in its ability to integrate distinct physical quanti-

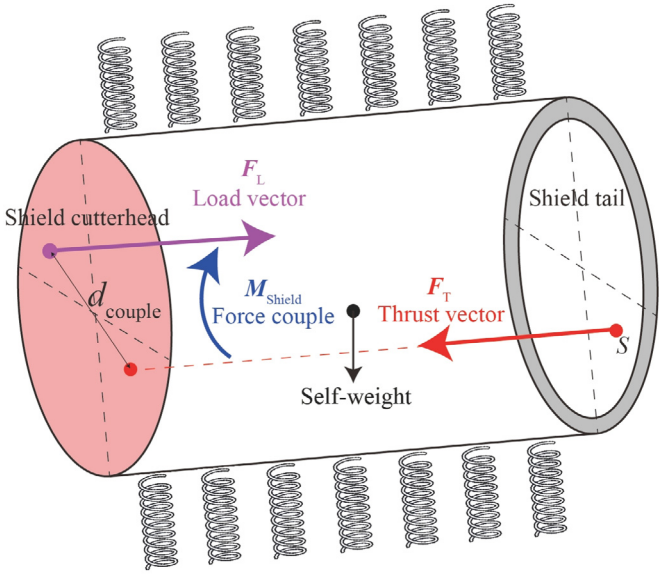

Fig. 6. Illustration of the dual-vector motion control mechanism.

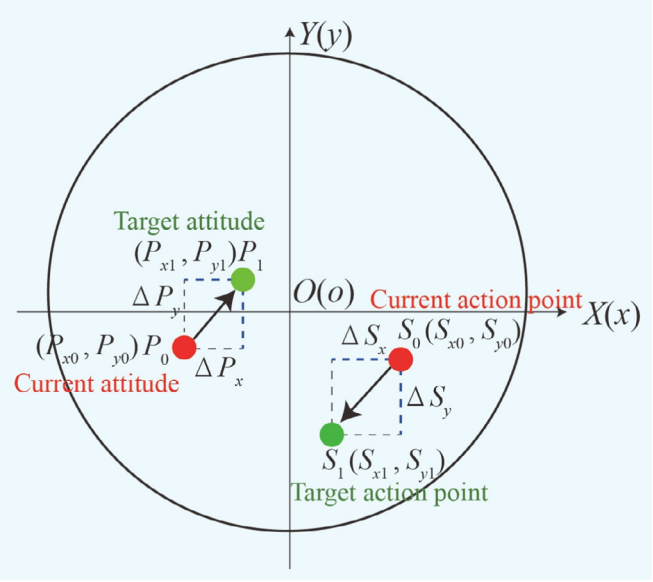

Fig. 7. Interaction between the shield thrust action point and shield attitude point.

ties within a unified control framework, thereby enabling the formation of a closed-loop control system. The effectiveness of PID control in the attitude regulation of thrust-vectoring aircraft is largely attributed to its capacity to capture and leverage the strong correlation between changes in fuselage orientation and the resulting thrust torque (Zhen et al., 2024).

It is worth noting that the shield attitude angle deviations (θ_x in the horizontal direction and θ_y in the vertical direction) are adopted as the controlled state variables, replacing the previously used attitude deviations (P_x,P_y). This approach provides a more precise characterization of the spatial orientation of the entire shield machine, as it simultaneously considers the attitudes of both the shield cutterhead and tail. The calculations for θ_x and θ_y (see Fig. 8) are as follows:

$$\theta_x = \frac{P_{x\_head} - P_{x\_tail}}{l}, \tag{7}$$

$$\theta_y = \frac{P_{y\_head} - P_{y\_tail}}{l}, \tag{8}$$

where l stands for the length of the shield machine, P_{x_head} and P_{x_tail} are the attitude deviations of the shield cutterhead and shield tail in the horizontal direction, respectively, while P_{y_head} and P_{y_tail} are the attitude deviations of the shield cutterhead and shield tail in the vertical direction, respectively.

We apply the control law to shield tunnel construction and develop a parallel PID control system for the automatic regulation of shield attitude and speed, as illustrated in Fig. 9. Specifically, the system includes three controllers: the first controller uses the target steering angle in the horizontal direction as the input signal and outputs the corresponding target horizontal thrust force moment; the second one uses the target steering angle in the vertical direction as the input signal and outputs the corresponding target vertical thrust force moment; and the third one takes the target shield speed as the input signal and outputs the corresponding target thrust force. These three PID controllers operate in parallel to determine the final target thrust vector, which is then executed by the control system.

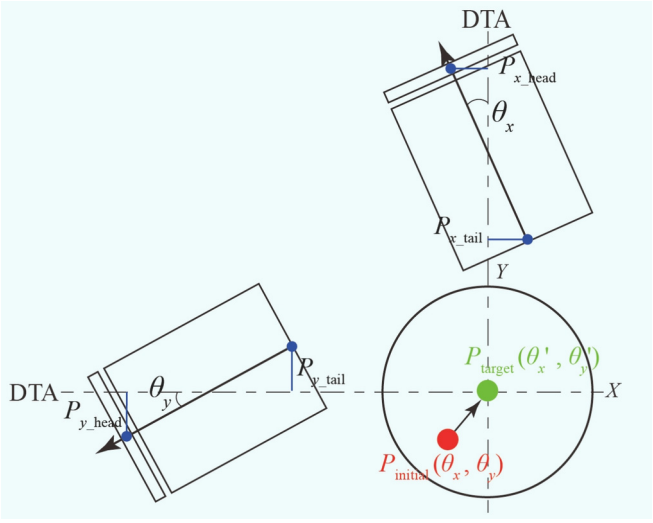

Fig. 8. Definition of shield attitude angle deviation ($P_{initial}$ and P_{target} are the initial and target attitude angle deviation points, respectively).

However, due to the multiphase nature and inherent uncertainty of geotechnical media, the attitude control of shield machines is fundamentally different from that of aviation systems. The shield machine, surrounded by soils and rocks, exhibits a significantly lower response sensitivity compared to aircraft. Consequently, once the shield attitude deviates, a considerable tunneling distance is required for attitude correction. During this correction process, the safety of both the tunneling equipment and the surrounding environment must be carefully considered. As a result, it is widely acknowledged that achieving millimeter-level precision in controlling the attitude of a machine with thrust forces reaching thousands of tons is an immense challenge.

In summary, the core contributions of this paper focus on two key aspects: determining the target steering angles of the shield machine and generating and executing the corresponding target thrust vectors.

3.3 Generation method for target steering angles

3.3.1 Calculation method of regression distance

In general, due to the inevitable solidification time of the synchronous grouting slurry, the assembled segmental rings tend to experience vertical displacement (primarily uplift, though occasional settlement may occur) after detaching from the shield tail. To meet tunnel construction acceptance standards, the primary objective of shield attitude control is to position the segmental rings within an allowable range near the DTA following any horizontal or vertical displacement (see Fig. 10(a) and (b)). To facilitate this, we introduce the concept of construction tunnel axis (CTA) to represent the position where the shield tail should ideally be located (see Fig. 10(c)). The CTA is parallel to the DTA in the 3D space. As illustrated in Fig. 10 (c), a control point can be freely selected on the shield body, simplifying the shield machine to a vector (i.e., a directed line segment originating from the control point). In this study, the control point was selected at the center of the shield cutterhead and was subsequently used for motion path planning and trajectory formation.

As shown in Fig. 11, practical experience indicates that shield machines tend to adopt specific attitudes once they enter stable tunneling conditions. These attitudes are typically used as control targets after the shield machine has traveled a certain regression distance, i.e., the shield machine reaches the CTA after advancing a specific distance from its deviation relative to the CTA.

This paper proposes a method for determining the regression distance based on the construction experience of our research team. The calculation methods for both the horizontal and vertical directions are consistent, with the larger value being adopted. Taking horizontal shield

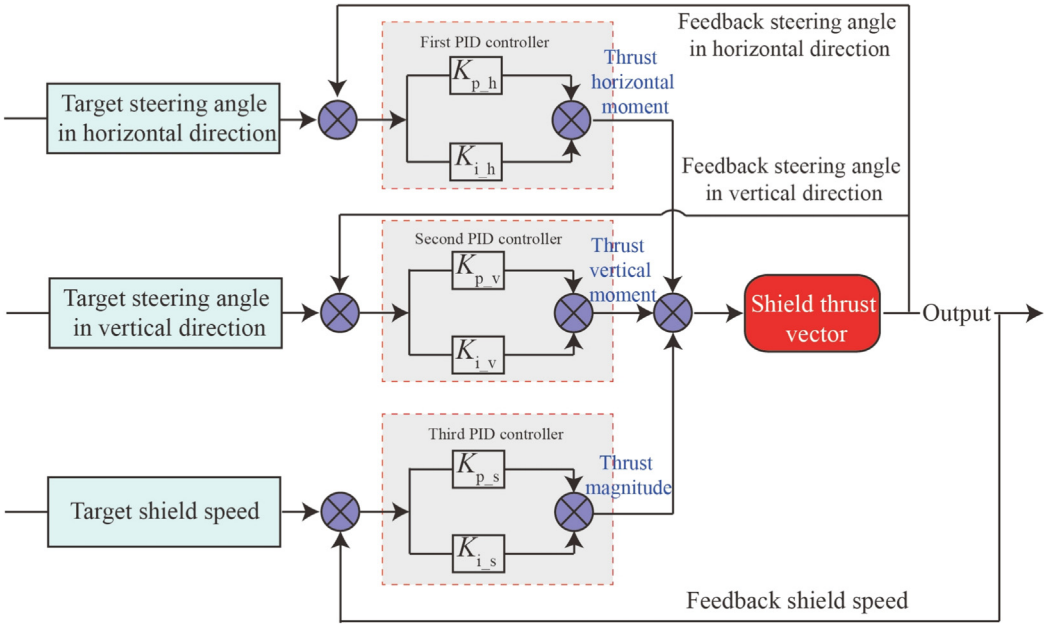

Fig. 9. Parallel PID control system (K_{p_h} and K_{p_v} are the proportional coefficients in the horizontal and vertical direction for attitude control, respectively; K_{i_h} and K_{i_v} are the integral coefficients in the horizontal and vertical direction for attitude control, respectively; K_{p_s} and K_{i_s} are the proportional and integral coefficients for speed control, respectively).

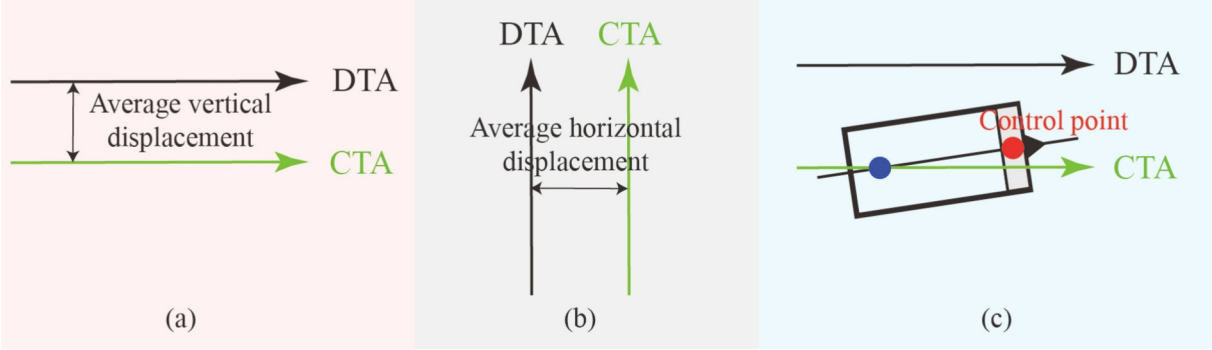

Fig. 10. Definition of CTA and control point. (a) Vertical direction, (b) horizontal direction, and (c) control point and preset attitudes.

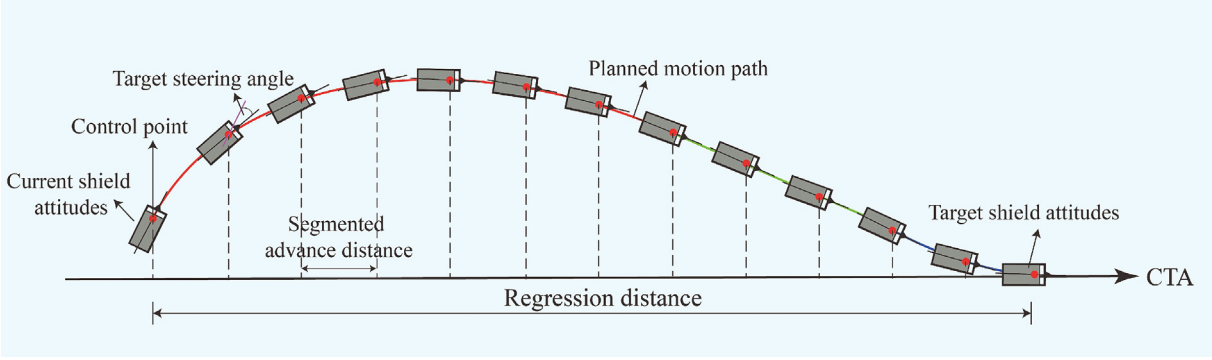

Fig. 11. Schematic diagram of motion path planning.

attitude control as an example, the safety threshold and warning threshold for the attitude deviation of the control point relative to the CTA are set to m_1 and m_2, respectively. The regression distance s, which is primarily determined by the attitude deviation of the control point m_0 and the motion trend of the shield machine relative to the CTA,

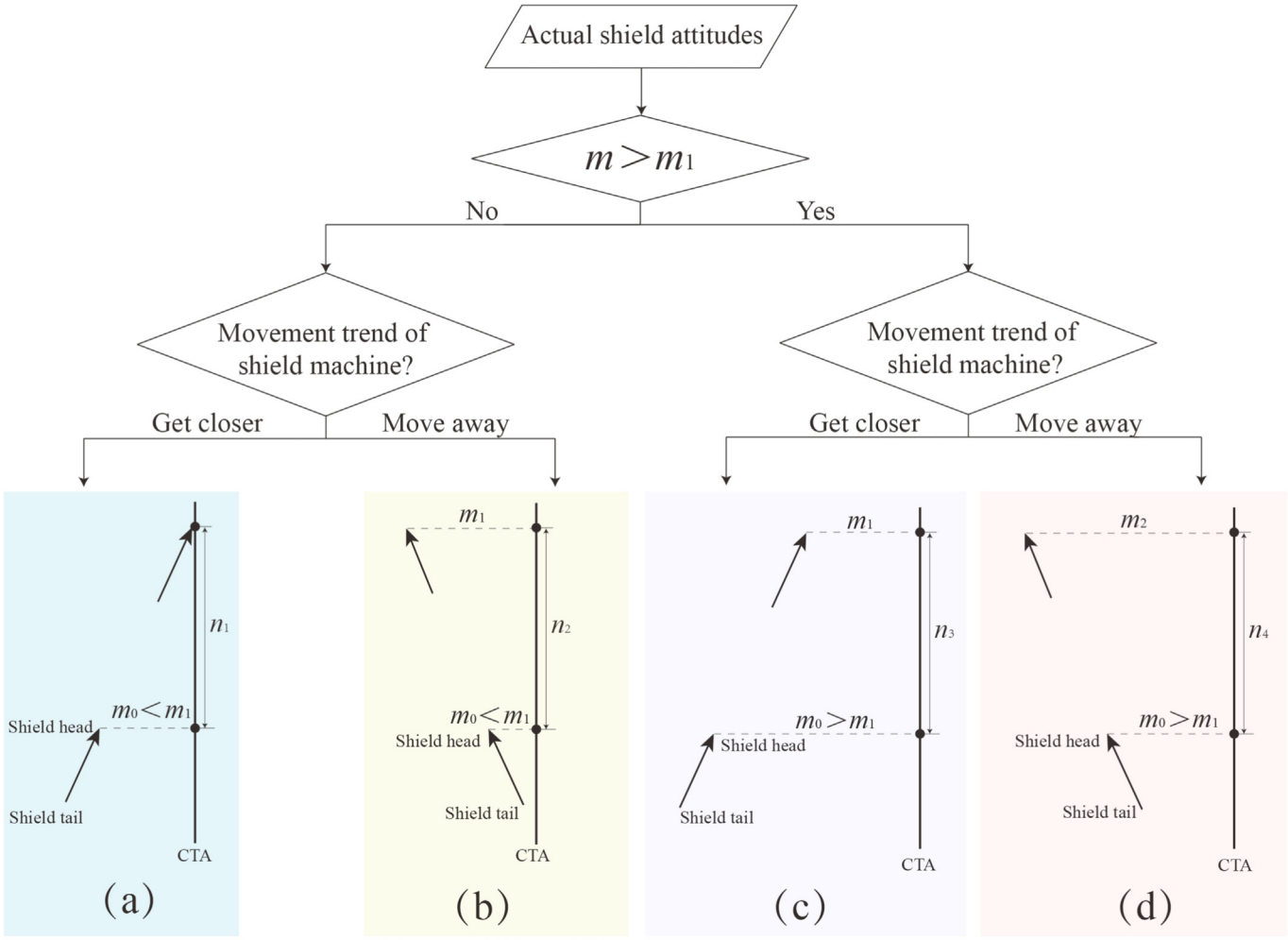

Fig. 12. Calculation flow chart of regression distance.

can be calculated as shown in Fig. 12. The specific calculation process is detailed as follows.

Determine whether the attitude deviation of the control point relative to the CTA m_0 exceeds m_1.

If not, further assess whether the motion path of the shield machine, while maintaining its current attitude and advancing forward, will intersect with the CTA.

If the assessment result is affirmative, calculate the distance n_1 between the current projection of the control point onto the CTA and the point of intersection (Fig. 12(a)). If $n_1 > l$, set $s = l$; if $n_1 \leq l$, set $s = n_1$.

If the assessment result is negative, locate the final projection of the control point on the CTA when the attitude deviation reaches m_1, and calculate the distance n_2 between the current and final projections (Fig. 12(b)). If $n_2 > 5$, set $s = l$; if $n_2 \leq 5$, set $s = l + 5 - n_2$.

If m_0 exceeds m_1, assess whether the motion path of the shield machine, while maintaining its current attitude and advancing forward, will intersect with the CTA.

If the assessment result is affirmative, locate the final projection of the control point on the CTA when the attitude deviation reaches m_1, and calculate the distance n_3 between the current and final projections (Fig. 12(c)). If $n_3 > l$, set $s = 2l$; if $n_3 \leq l$, set $s = l + n_3$.

If the assessment result is negative, locate the final projection of the control point on the CTA when the attitude deviation reaches m_2, and calculate the distance n_4 between the current and final projections (Fig. 12(d)). If $n_4 > 5$, set $s = 2l$; if $n_4 \leq 5$, set $s = 3l - n_4$.

In addition to shield attitudes, the effect of the shield tail clearance is also considered in the calculation of the regression distance.

If the current minimum shield tail clearance exceeds half of the safety threshold, its impact on the regression distance can be neglected.

If the current minimum shield tail clearance is less than half of the safety threshold and exhibits a decreasing trend, the number of segmental rings required to adjust the shield tail clearance, denoted as T, is set to 3.

If the current minimum shield tail clearance is less than half of the safety threshold but is trending upward, T is set to 2.

The regression distance D, which accounts for both shield attitudes and shield tail clearance, can then be calculated using the following formula:

$$D = k\left(s + d_{\text{seg}} \times T\right), \tag{9}$$

where k represents the influence parameter of geological conditions on the regression distance, determined based on actual construction conditions, and d_{seg} denotes the width of the segmental ring.

3.3.2 Motion path planning and navigation method

As illustrated in Fig. 13, three typical motion path types are utilized in practical applications of this technology, corresponding to different scenarios in both the horizontal and vertical directions. During the design phase, various trajectory types, such as circular curves, cubic polynomial curves, straight lines, and transition curves, can be selected and combined, provided that smooth transitions between different curve types are maintained.

The design of the cubic polynomial curve motion path is illustrated in Fig. 14 to demonstrate the generation of target steering angles, and the function expression is provided below.

$$y = a_0x^3 + b_0x^2 + c_0x + d_0, \tag{10}$$

where a_0, b_0, c_0, and d_0 are the unknown coefficients to be determined.

The slope at any point on the cubic polynomial curve is given by

$$y' = 3a_0x^2 + 2b_0x + c_0. \tag{11}$$

The solution of all partial factors must satisfy the following four conditions:

$$\text{When } x = 0,\ y = m_0, \tag{12}$$

$$\text{When } x = D,\ y = 0, \tag{13}$$

$$\text{When } x = 0,\ y' = 3a_0x^2 + 2b_0x + c_0 = \tan\psi, \tag{14}$$

$$\text{When } x = D,\ y' = 3a_0x^2 + 2b_0x + c_0 = 0, \tag{15}$$

where Ψ is the attitude angle deviation relative to CTA at the starting point of the motion path.

As shown in Fig. 11, the motion path is divided into segments, and the target steering angle in the horizontal or vertical directions for each segment can be calculated and then provided. Ultimately, the target steering angle of the shield machine $\Delta\varphi$ for each segment can be expressed as

$$\Delta\varphi = \left|\arctan Y_1' - \arctan Y_0'\right|, \tag{16}$$

where Y_1' and Y_0' represent the slope values at the start and end points of each segmented advance distance, respectively.

3.4 Automatic control of thrust vector

Thrust vectoring technology (Afridi et al., 2023; Invernizzi & Lovera, 2018; Invernizzi et al., 2020) was initially introduced in the aerospace sector during the 1970s, with the first vector-propelled aircraft developed in the 1990s. The core principle of this technology involves utilizing the thrust vector generated by the engine to produce additional control torque through nozzle deflection, thereby enabling precise attitude control and significantly enhancing aircraft maneuverability. In recent years, the thrust-vectoring technology has also witnessed rapid advancements in the field of naval engineering (Zhou & Zhao, 2020).

3.4.1 Control method of thrust vector

The construction scheme of shield tunneling is a periodic combination of downtime, initiation, and advancement, as shown in Fig. 15: the shield machine starts from a halted or paused state and keeps advancing until a predesigned excavation length is reached, followed by the downtime of the next excavation cycle. During the tunneling process, the shield thrust vector involves two key pieces of information:

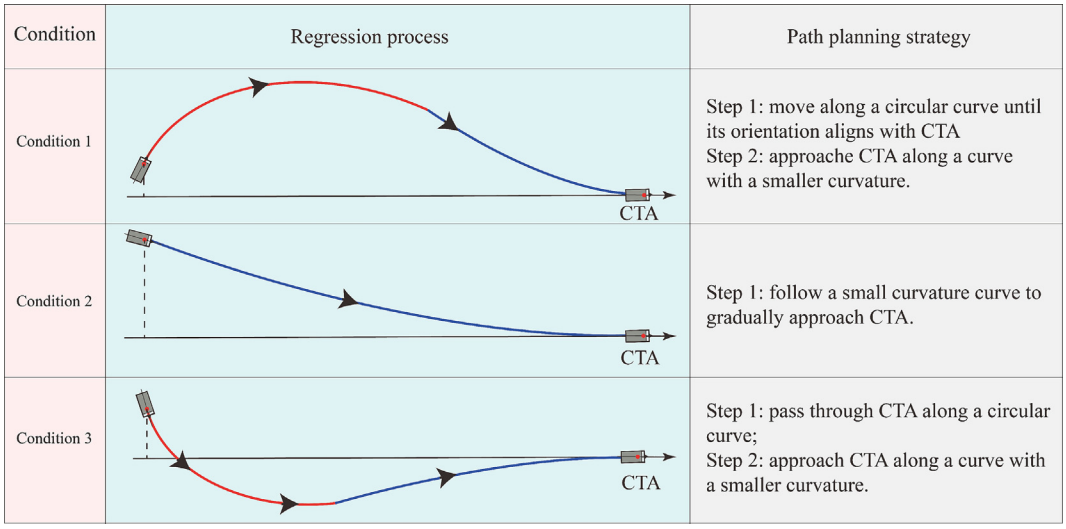

Fig. 13. Schematic diagram of motion path planning strategies.

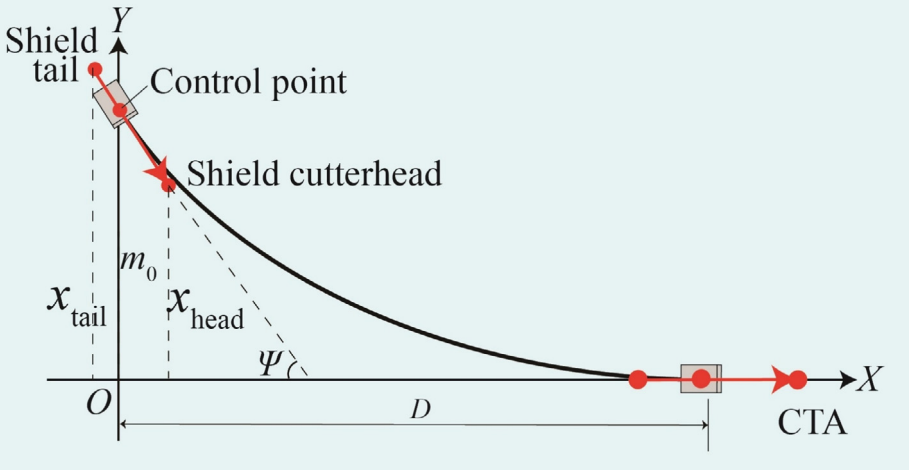

Fig. 14. Calculation diagram of motion path (cubic polynomial curve) (x_{head} and x_{tail} are the attitude deviations of the shield cutterhead and shield tail, respectively).

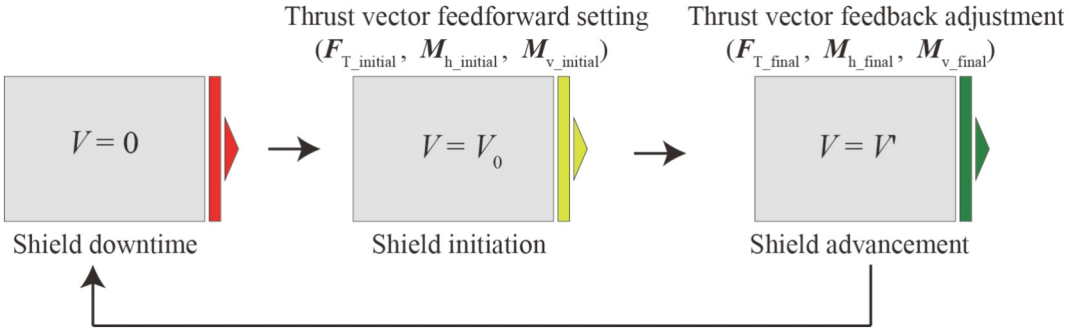

Fig. 15. Schematic for the cycle of shield tunneling process (V is the shield speed, V_0 and V' stand for the initial and adjusted speeds, respectively).

thrust force and the location of thrust action point. The former ensures the uniform advancement of the shield machine, while the latter determines its steering ability. In this paper, the control of the thrust vector includes two technologies: feedforward setting and feedback adjustment. The former is to start the shield machine based on geotechnical theory, and the latter is driven by the improved PID control law (Section 3.2) to maintain the tunneling speed and correct the shield attitudes.

The general process of thrust vector feedforward calculation ($\boldsymbol{F}_{T\_initial}$, $\boldsymbol{M}_{h\_initial}$, and $\boldsymbol{M}_{v\_initial}$) is shown in Fig. 16, and for a detailed explanation of the method, please refer to reference (Xie et al., 2024); it will not be reiterated here.

From a control perspective, regulating the thrust force is relatively straightforward. After the shield machine is initiated using the thrust vector feedforward results ($\boldsymbol{F}_{T\_initial}$, $\boldsymbol{M}_{h\_initial}$, and $\boldsymbol{M}_{v\_initial}$), the driving speed is continuously monitored in real time. If the shield's advancement speed drops by 5 mm/min, the target thrust force is increased at a rate of 1% per second, based on the current thrust force $\boldsymbol{F}_{T\_initial}$, until the shield speed recovers to the predefined setpoint. Once the shield speed reaches and stabilizes at the desired value, the latest target thrust force $\| \boldsymbol{F}_{T\_final} \|$ ($\| \boldsymbol{F}_{T\_final} \| = \| \boldsymbol{F}_{T\_initial} \| + \Delta F$) is held constant.

During this adjustment process, as detailed in Section 2.1, the differential flow rates between the slurry supply and discharge (or the rotational speed of the screw conveyor) are automatically controlled through a closed-loop feedback system. This ensures that the pressure within the slurry chamber (or soil chamber) is maintained at the specified setpoint.

Referring to Figs. 8 and 9, the control law equations for feedback adjustment of thrust action point displacements in both directions (ΔS_x and ΔS_y) are expressed as follows.

$$\Delta S_x = K_{p\_h}\Delta\theta_x(t) + K_{i\_h}\int_0^t \Delta\theta_x(t)\mathrm{d}t, \tag{17}$$

$$\Delta S_y = K_{p\_v}\Delta\theta_y(t) + K_{i\_v}\int_0^t \Delta\theta_y(t)\mathrm{d}t, \tag{18}$$

where K_{p_h} and K_{p_v} are the proportional coefficients in the horizontal and vertical direction, respectively; K_{i_h} and K_{i_v} are the integral coefficients in the horizontal and vertical direction, respectively; t denotes the sampling period.

The four aforementioned control law coefficients are determined by a machine learning method, i.e., the ridge regression algorithm (Wang et al., 2022). Ridge regression is an improved least squares estimation method that

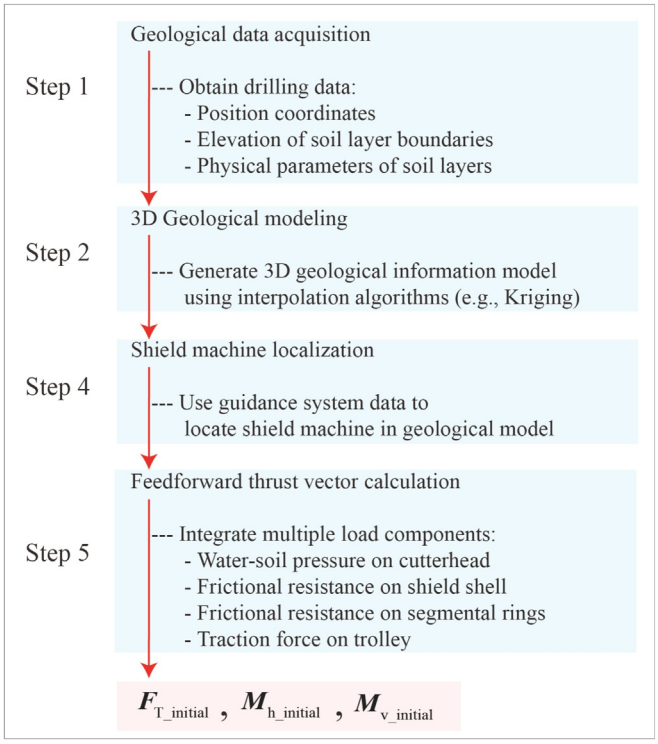

Fig. 16. Flowchart of thrust vector feedforward calculation.

sacrifices some accuracy by introducing bias, thereby reducing the sensitivity to multicollinearity and improving the model's robustness. This method is considered more practical and reliable than ordinary least squares, particularly in the presence of outliers, due to its enhanced fitting capability. The process for determining these coefficients is illustrated in Fig. 17 and explained as follows.

Given a sample x described by d-dimensional attributes $(x_1, x_2, x_3, \cdots, x_d)$, where x_i represents the value of the i-th dimensional attribute of sample x. The linear model can be expressed as

$$f(x) = \omega_1 x_1 + \omega_2 x_2 + \cdots + \omega_d x_d + b, \tag{19}$$

where b is the bias term, and $\boldsymbol{\omega}$ represents the weight coefficients for each feature dimension. By solving for $\boldsymbol{\omega}$ and b, the final model is determined. In practical applications, the bias term is often set to zero.

From a geometric perspective, the least squares method is used to solve this linear regression problem by minimizing the loss function $L(\boldsymbol{\omega})$, where $L(\boldsymbol{\omega})$ is defined as

$$L(\boldsymbol{\omega}) = \sum_{i=1}^{N} \|\boldsymbol{\omega}^{\mathrm{T}} x_i - y_i\|^2, \tag{20}$$

where N is the number of samples.

Let $\boldsymbol{X}$ be the matrix of multiple samples, and $\boldsymbol{Y}$ be the corresponding output of the linear model, then, equation (19) can be transformed as

$$\boldsymbol{Y} = \boldsymbol{X}\boldsymbol{\omega} + b. \tag{21}$$

In matrix form, the loss function can be rewritten as

$$L(\boldsymbol{\omega}) = \boldsymbol{\omega}^{\mathrm{T}}\boldsymbol{X}^{\mathrm{T}}\boldsymbol{X}\boldsymbol{\omega} - 2\boldsymbol{\omega}^{\mathrm{T}}\boldsymbol{X}^{\mathrm{T}}\boldsymbol{Y} + \boldsymbol{Y}^{\mathrm{T}}\boldsymbol{Y}. \tag{22}$$

To find the optimal $\boldsymbol{\omega}$, take the derivative of $L(\boldsymbol{\omega})$ with respect to $\boldsymbol{\omega}$ and equate it to zero. This gives the closed-form solution for $\boldsymbol{\omega}$:

$$\hat{\boldsymbol{\omega}} = \left(\boldsymbol{X}^{\mathrm{T}}\boldsymbol{X}\right)^{-1}\boldsymbol{X}^{\mathrm{T}}\boldsymbol{Y}. \tag{23}$$

Ridge regression extends the linear regression model by adding an L2 regularization penalty term, which helps to prevent overfitting by penalizing large coefficient values. The modified loss function is expressed as

$$p(\boldsymbol{\omega}) = L(\boldsymbol{\omega}) + \lambda\|\boldsymbol{\omega}\|_2, \tag{24}$$

where λ is the regularization parameter that controls the strength of the penalty. The larger the value of λ, the stronger the regularization effect. In the current model, we use the combination of cross validation and empirical estimation to determine λ.

By solving the ridge regression loss function, the weight vector $\boldsymbol{\omega}$ can be computed as

$$\boldsymbol{\omega} = \left(\boldsymbol{X}^{\mathrm{T}}\boldsymbol{X} + \lambda\boldsymbol{I}\right)^{-1}\boldsymbol{X}^{\mathrm{T}}\boldsymbol{Y}, \tag{25}$$

where $\boldsymbol{I}$ is the identity matrix.

Furthermore, the moments of thrust force in the horizontal and vertical directions (M_{h_final} and M_{v_final}) can be adjusted based on the feedforward calculation results and are expressed as

$$M_{h\_final} = \| \boldsymbol{F}_{T\_final} \|(S_{x0} + \Delta S_x), \tag{26}$$

$$M_{v\_final} = \| \boldsymbol{F}_{T\_final} \|(S_{y0} + \Delta S_y), \tag{27}$$

where S_{x0} and S_{y0} are the initial position coordinates of the thrust force.

3.4.2 Execution method of thrust vector

In this paper, the method for allocating the target thrust vectors (F_{T_final}, M_{h_final}, and M_{v_final}) generated by the automatic system to each propulsion cylinder is relatively straightforward, requiring only the satisfaction of a set of constraint equations. It is important to note that, unlike traditional shield propulsion systems, which are grouped into fixed zones, newly manufactured shield machines are capable of independent oil pressure control for each propulsion unit, allowing for flexible partitioning of the propulsion system. As an example, a three-zone configuration for the newly manufactured shield machine is illustrated in Fig. 18, which will be implemented in the subsequent demonstration project.

The shield propulsion system, consisting of multiple hydraulic cylinders, is divided into three zones, i.e., from Zone A–C. Zones A and B contain an equal number of propulsion cylinders, while the remaining cylinders are assigned to Zone C. It is required that the number of cylinders in Zone C be greater than that in either Zone A or Zone B. The target oil pressure within each zone is maintained uniformly across all cylinders. The configuration

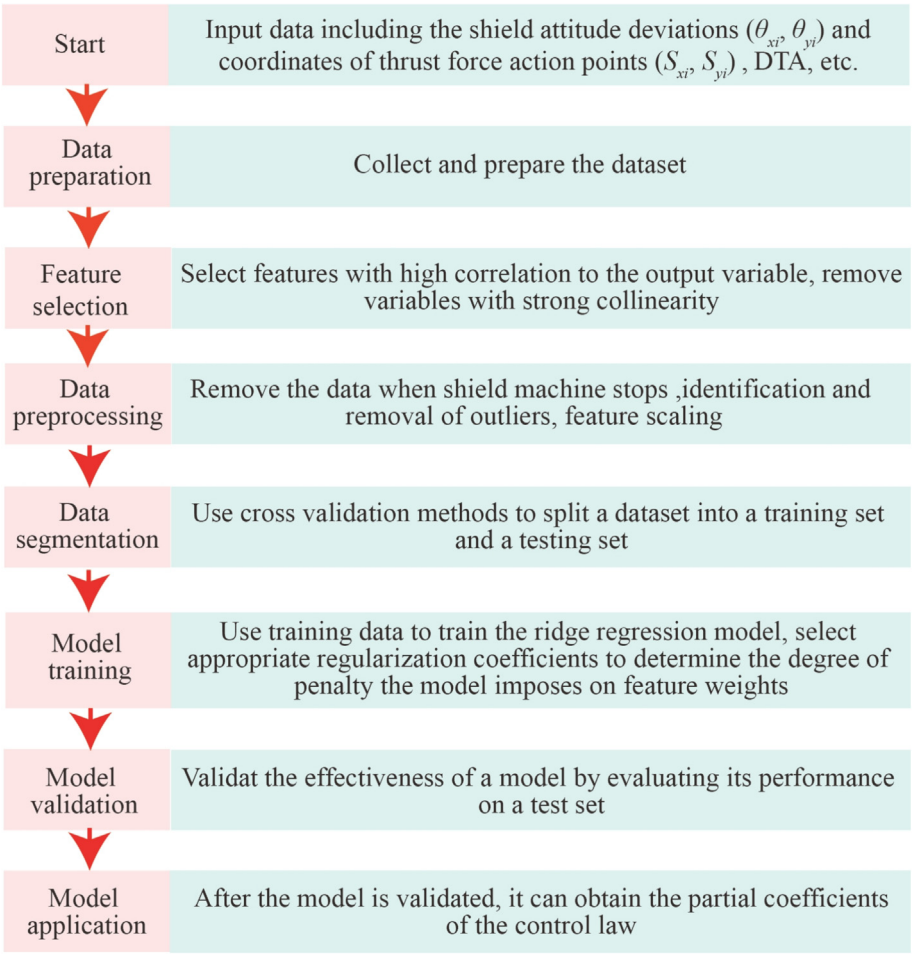

Fig. 17. Flowchart of ridge regression algorithm.

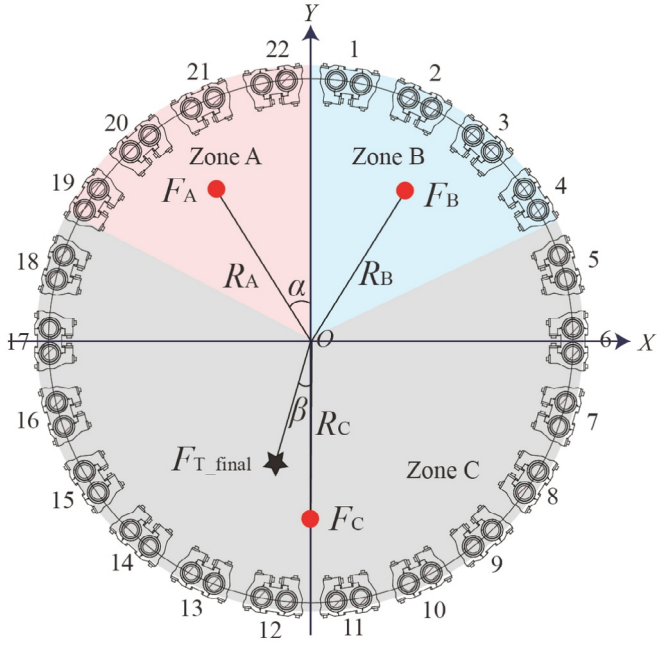

Fig. 18. Schematic diagram of the distribution of the target thrust vector.

of the three zones dynamically adjusts in response to changes in the position of the target thrust action point. The goal is to align the target thrust action point as closely as possible with the symmetry axis of Zone C. For a detailed explanation of this adjustment mechanism, please refer to Zhu et al. (2023), which will not be reiterated here. The target thrust for each zone is denoted as F_A, F_B, and F_C, and the unique solution for the thrust distribution can be determined from the following three constraint equations.

$$F_{T\_final} = F_A + F_B + F_C, \tag{28}$$

$$\sqrt{M_{h\_final}^2 + M_{v\_final}^2}\sin\beta = (F_A - F_B)R_A\sin\alpha, \tag{29}$$

$$\sqrt{M_{h\_final}^2 + M_{v\_final}^2}\cos\beta = F_C R_C - (F_A R_A + F_B R_B)\cos\alpha, \tag{30}$$

where α is the angle between the symmetry axis of Zones A and B and the positive half of the Y-axis, and β is the angle between the line connecting the thrust action point and the center of the propulsion system and the negative half of the Y-axis. R_A, R_B, and R_C denote the distances from the

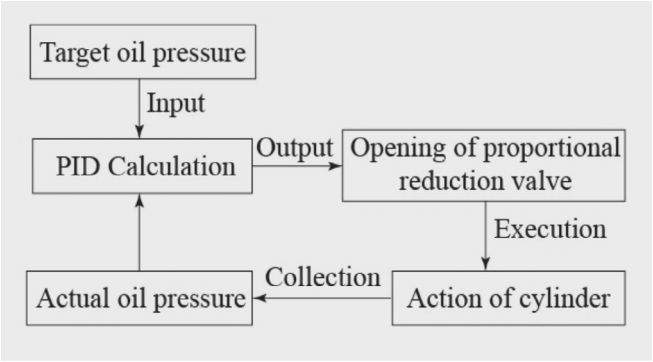

Fig. 19. Closed-loop execution principle of target oil pressure.

target thrust action points of Zones A, B, and C to the center of the propulsion system, respectively.

Once F_A, F_B, and F_C are determined, the average thrust per cylinder in each zone can be calculated and subsequently converted into the corresponding target oil pressure for each cylinder. The precise implementation of these target oil pressures will ensure the accurate realization of the desired thrust vector (see Fig. 19).

4 Large-scale model testing validation

4.1 Model test platform

As illustrated in Fig. 20, a super-large model test platform (13 m × 8 m × 8 m) mainly consisted of a steel outer frame, a load system, a model shield machine, a sliding support, and steel segments, which was established to verify the feasibility of this thrust-vectoring automatic shield tunneling technology. Two prisms, mounted on one side of the horizontal symmetry axis of the shield shell, are utilized to continuously measure the real-time attitude angle deviations of the shield machine (θ_x and θ_y) and the attitude deviations of the shield cutterhead (P_x and P_y).

The load system consisted of 6 groups of dual hydro-cylinders evenly distributed around the circumference with a diameter of 3.6 m. The inner diameter of the load hydro-cylinder, the diameter of the piston-rod, and the maximum cylinder stroke were 360, 280, and 3000 mm, respectively. Each thrust unit was equipped with an independent proportional reduction valve for pressure control, and it could actively output non-constant load vectors (with a maximum load capacity of 1.38×10^4 kN) to simulate various load conditions encountered by the shield machine.

A real metro shield machine with a diameter of approximately 6.8 m was innovatively modified by removing components such as the cutter head, front shield, and shield tail, while retaining the middle shield, propulsion system, and segment erector. A load-bearing circular ring was installed at the front of the model shield machine to support the jacks of the loading system. The model shield machine has a total length of approximately 5.7 m and a total weight of about 1.60×10^5 kg, with the propulsion system consisting of 17 groups of dual hydro-cylinders. The inner diameter of the propulsion hydro-cylinder, diameter of the piston-rod, and maximum of the cylinder stroke were 240, 200, and 2200 mm, respectively. An independent proportional reduction valve was employed to achieve closed-loop control of the target oil pressure for each group of dual hydro-cylinders, which was also equipped with an oil pressure sensor and a travel sensor. The cylinder stroke sensor model is BTL5-S111B-M2450-K-K15 (resolution: 5×10^{-6} m), and the pressure sensor model is MBS3050-060G3583 (resolution: 0.4 MPa).

It is important to note that, due to practical constraints, it was unable to embed this oversized testing platform into the soil. To increase the test difficulty, a hemispherical single-point contact was established between the model shield machine and the sliding support, which constrains the vertical displacement of the model shield machine only, leaving other degrees of freedom to remain unconstrained. This design aims to maximize the response of the shield attitude to assess the feasibility of this technology. The detailed introduction about the testing platform, as well as the calculation methods for the distribution of the set load force vectors and thrust vectors to each group of dual hydro-cylinder, could also be referred to Zhu et al. (2023).

Then, PID control law equations for the model test are established as follows, based on Fig. 9.

$$\Delta S_x = K_{p1}\Delta\theta_x(t) + K_{i1}\int_0^t \Delta\theta_x(t)\mathrm{d}t, \tag{31}$$

$$\Delta S_y = K_{p1}\Delta\theta_y(t) + K_{i1}\int_0^t \Delta\theta_y(t)\mathrm{d}t, \tag{32}$$

$$\Delta F = K_{p2}\Delta V(t) + K_{i2}\int_0^t \Delta V(t)\mathrm{d}t, \tag{33}$$

where K_{p1} and K_{p2} are the proportional coefficients; K_{i1} and K_{i2} are the integral coefficients; ΔF is the increment of thrust force, $\Delta V(t)$ is the shield speed deviation, $\Delta\theta_x(t)$ is the attitude angle deviation in the horizontal direction, and $\Delta\theta_y(t)$ is the attitude angle deviation in the vertical direction.

Due to the relatively simple and controllable environmental conditions in this model test, the two proportional coefficients (K_{p1} and K_{i1}) in the shield attitude PID control law equations were subject to repeated tuning and validation. The final tuned values for these coefficients were determined to be 1000 and 10, respectively. Similarly, the coefficients K_{p2} and K_{i2} for speed control were set to 50 and 0, respectively. The sampling period employed in the control system was 5 ms.

4.2 Model test scheme

The variation in geological loads is indirectly replicated through active control of the load vector applied by the loading system, given that the rotation angle of the model shield machine can only undergo minimal changes. To

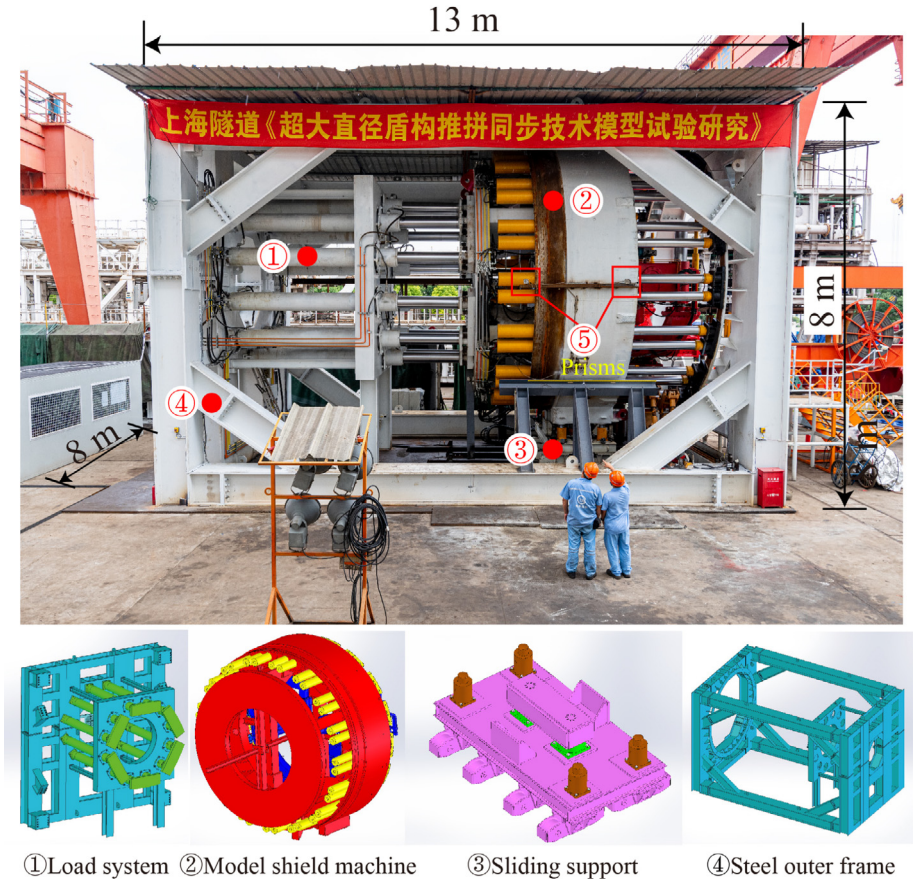

Fig. 20. Model test platform.

rigorously evaluate the feasibility of the proposed technology, simulations of uniform linear shield advancements with zero attitude angle deviations in both the horizontal and vertical directions were performed. These simulations aimed to assess the self-adaptive response of the shield thrust vector, which is generated by the automatic control system. To ensure the operational safety and stability of the tunneling process, the driving speed of the model shield machine was precisely controlled at approximately 15 mm/min throughout the test. Additionally, the contact interface between the sliding support located at the base of the shield machine and the ground sliding rail, along with the auxiliary anti-rollover brackets mounted on both sides of the shield machine, was meticulously designed to ensure the stability and safety of the shield's advancement.

The following two test scenarios are considered with the procedure designed as shown in Fig. 21. Test scenarios 1 and 2 aim to validate the correction control capability of the shield machine at the same burial depth and varying burial depths.

4.3 Data analysis

4.3.1 Analysis of the results from test scenario 1

Figure 22 illustrates the comparison of horizontal coordinates of thrust and load force action points throughout the entire process. During Phase 1, the load force vector remained stable, and the horizontal coordinates of the thrust action point exhibited a high degree of alignment with those of the load force. This consistency can be attributed to the manual operation of the propulsion system, which maintained the shield attitude in a nearly unchanged state.

In Phase 2, the horizontal attitude deviations of the shield cutterhead responded promptly to changes in the load force action point, as the propulsion system was no longer under manual control. As shown in Fig. 22, the model shield machine initially rotated to the right, followed by a rotation to the left. However, due to the prolonged duration of the horizontal moment at 1000 kN·m, the initial rightward displacement (+7 mm) was smaller than the subsequent leftward displacement (–19 mm). By the end of Phase 2, the horizontal attitude deviation reached –12 mm.

Upon entering Phase 3, the thrust-vectoring automatic control system was activated. It was observed from Fig. 22 that the coordinates of the thrust action point quickly increased to approach those of the load force action point, and after oscillating for approximately 30 s, gradually converged to a stable value. During this oscillation period, the amplitude of the coordinates of the thrust action point decreased progressively until it overlapped

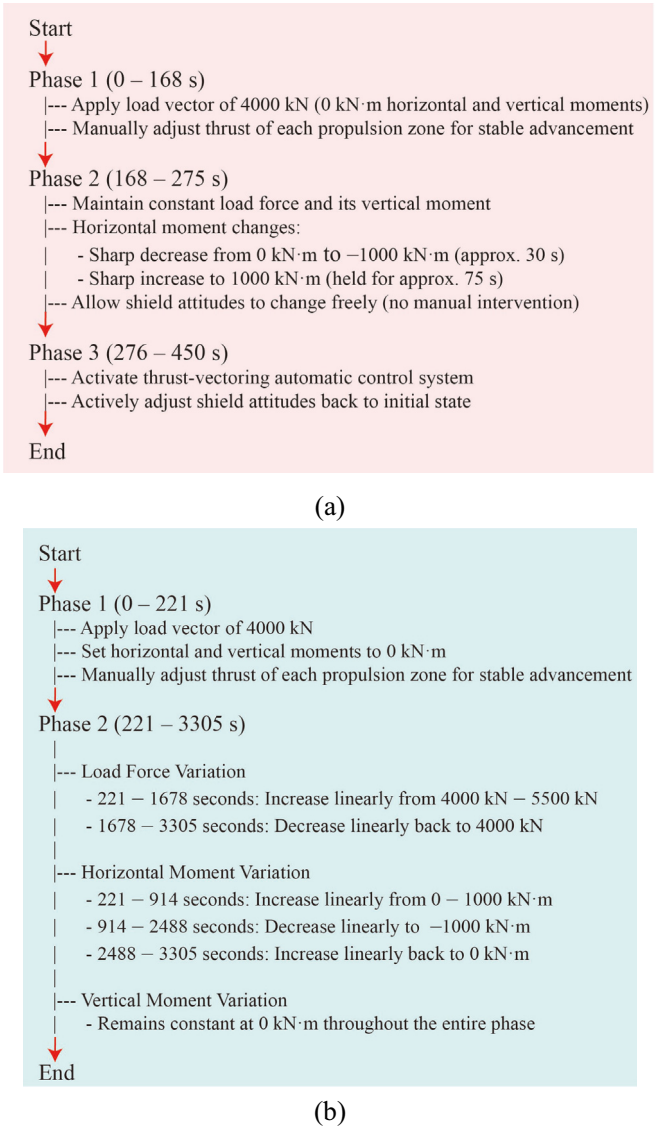

Fig. 21. Procedure design for both test scenarios. (a) Test scenario 1, and (b) test scenario 2.

with those of the load force action point. As shown in Fig. 22, the shield attitude steadily returned to its initial state, with a final deviation in the range of –1 to –3 mm.

4.3.2 Analysis of the results from test scenario 2

Test scenario 2 simulated an extreme working condition for the model shield machine, in which both the load force and its horizontal moment followed distinct variation paths simultaneously. The target shield speed and horizontal attitude deviation of the shield cutterhead were set to 13 mm/min and –2 mm, respectively. As shown in Figs. 23 and 24, the thrust vector (comprising the thrust force and horizontal coordinates of its action point) responded effectively to variations in the load force vector, maintaining a high degree of cooperativity throughout the process.

More specifically, a consistent deviation of approximately 1000 kN existed between the two forces due to system friction. A small amplitude fluctuation in the horizontal coordinates of the thrust action point was observed; however, no delayed response or significant overshoot occurred. Owing to the excellent adaptive response capability of the thrust vector, the overall shield speed of the model shield machine was maintained within an error range of –1 to +2 mm/min relative to the set value (see Fig. 23), while the horizontal attitude deviation of the shield cutterhead was controlled within an error range of ±3 mm (see Fig. 23).

In conclusion, the results of these two tests preliminarily demonstrate the feasibility of thrust-vectoring automatic shield tunneling technology in achieving precise adjustments of shield attitude and shield speed. This provides a solid foundation for the potential application of this technology in future practical engineering projects. However, due to limitations in the experimental conditions, this model test could not cover all the special working conditions that may be encountered in practical engineering applications, e.g., the impact of poorly set synchronous grouting parameters, which may lead to tail uplift issues affecting the application efficacy of this technology.

5 Practical application in engineering project

5.1 Project overview

Shanghai-Nantong Railway is a double-track high-speed railway that connects Shanghai with Nantong, a city in Jiangsu Province, China. As illustrated in Fig. 25, Wusongkou Yangtze River Tunnel spans a total length of 7.275 km. The main shield tunnel extends for a length of 6.77 km and is a double-bore, single-track underwater tunnel with segmental rings measuring 2 m in width. A total of 3385 segmental rings were used in the construction.

The stratigraphic distribution of the entire shield section, as shown in Fig. 26, belongs to a typical soft soil layer. The land segment is 1871 m long and primarily traverses the following strata: ②$_3$ silty clay, ③$_2$ silt sand, ④ silty clay, ⑤$_1$ clay, and ⑤$_2$ silt. The river crossing segment is 4799 m long and primarily traverses the following strata: ⑤$_1$ clay, ⑤$_2$ silt, ⑤$_{3\text{-}1}$ silty clay, and ⑤$_{3\text{-}11}$ silt layer. The tunnel features a maximum longitudinal gradient of 9.0‰ and a minimum turning radius of 778 m. The overburden thickness ranges from a minimum of 6.26 m to a maximum of 29.2 m.

Two domestically manufactured shield machines, as shown in Fig. 27, each with an excavation diameter of 10.69 m, commence tunneling from Working Shaft No. 3 in Pudong New District, crossing the Huangpu River and the Yangtze River in succession, before being received at Working Shaft No. 2 in Baoshan District. The maximum driving speed of the shield machine is 80 mm/min, with a maximum working pressure of 0.8 MPa. The total power of the main drive is 2400 kW, and the rated torque is 22 950 kN·m. The propulsion system of the shield machine consisted of 22 groups of dual hydro-cylinders evenly dis-

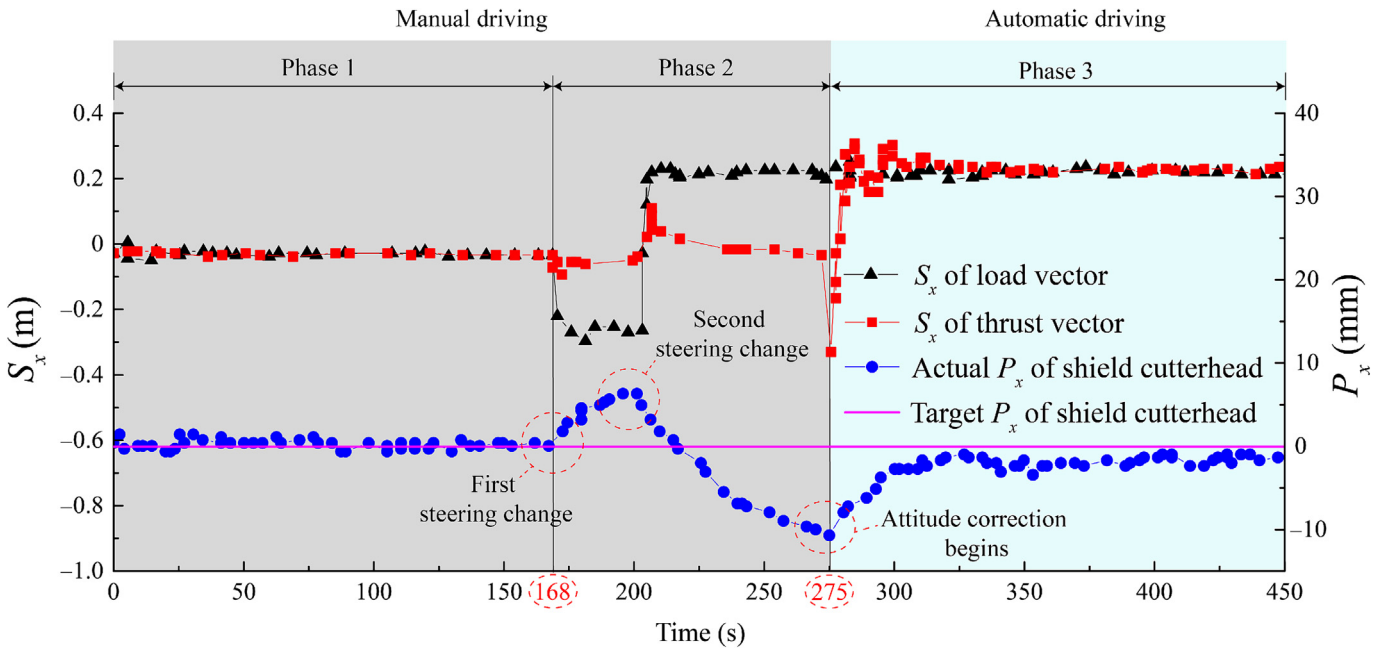

Fig. 22. Variations in the horizontal coordinates of thrust and load action points, and changes in shield attitude in test 1.

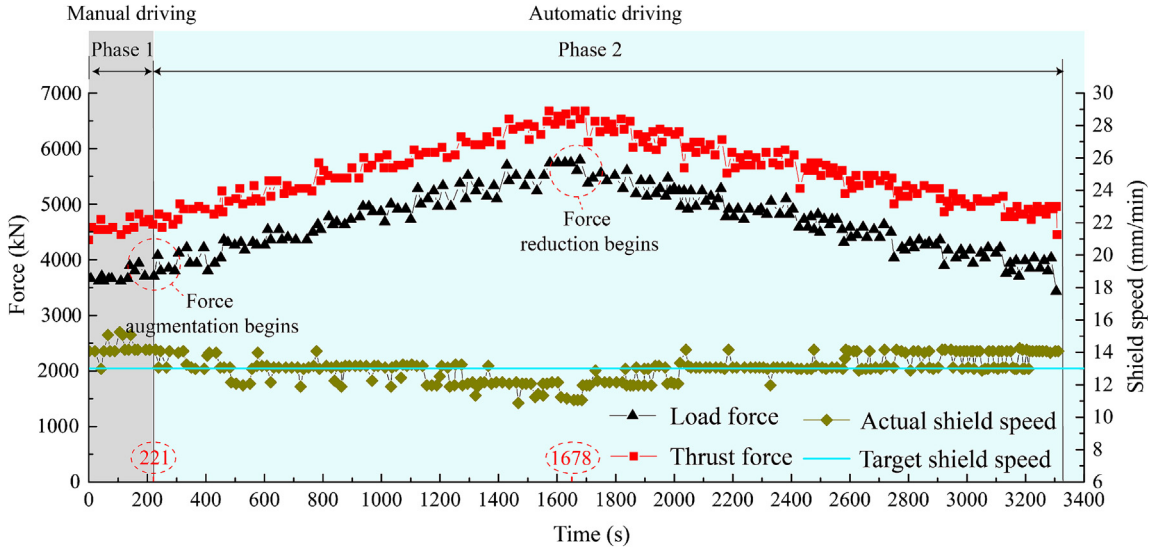

Fig. 23. Variations in thrust, load forces, and shield speed in test scenario 2.

tributed around the circumference with a total thrust of 139 800 kN. The inner diameter of the hydraulic cylinder, and the diameter of the piston-rod were 340 and 260 mm, respectively. All the dual hydro-cylinders were controlled independently, and the pressure distribution method for each hydro-cylinder based on the target total thrust vector has been explained in Section 3.4.2.

The thrust-vectoring automatic shield tunneling technology was first implemented on the right line of Wusongkou Yangtze River Tunnel project. During the initial application of this technology, to achieve gradual correction of the shield attitude, the target steering angles provided by the path planning module were relatively small, which did not meet the shield operator's habitual need for quick corrections. This occasionally led to manual overrides of the system. After repeated technical discussions, the psychological concerns of the shield operators were addressed. Construction commenced in March 2023 and was completed in January 2024. Algorithm debugging took place between the 385th and 633rd rings, while the demonstration phase was carried out from the 634th ring to the 3261st ring, covering a total of 2628 rings, which accounts for 77.6% of the tunnel's total length. Among these, 396 segmental rings (792 m, from the 2866th ring to the 3261st ring) were continuously and automatically controlled for shield attitude. Notably, a world record for

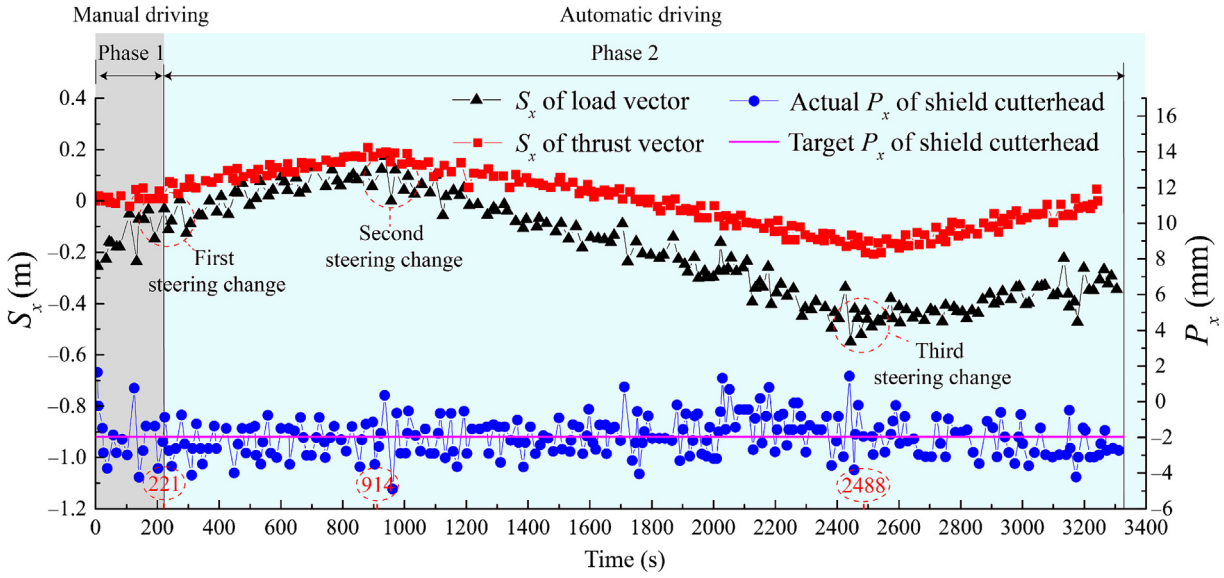

Fig. 24. Variations in the horizontal coordinates of thrust and load action points, and changes in shield attitude in test scenario 2.

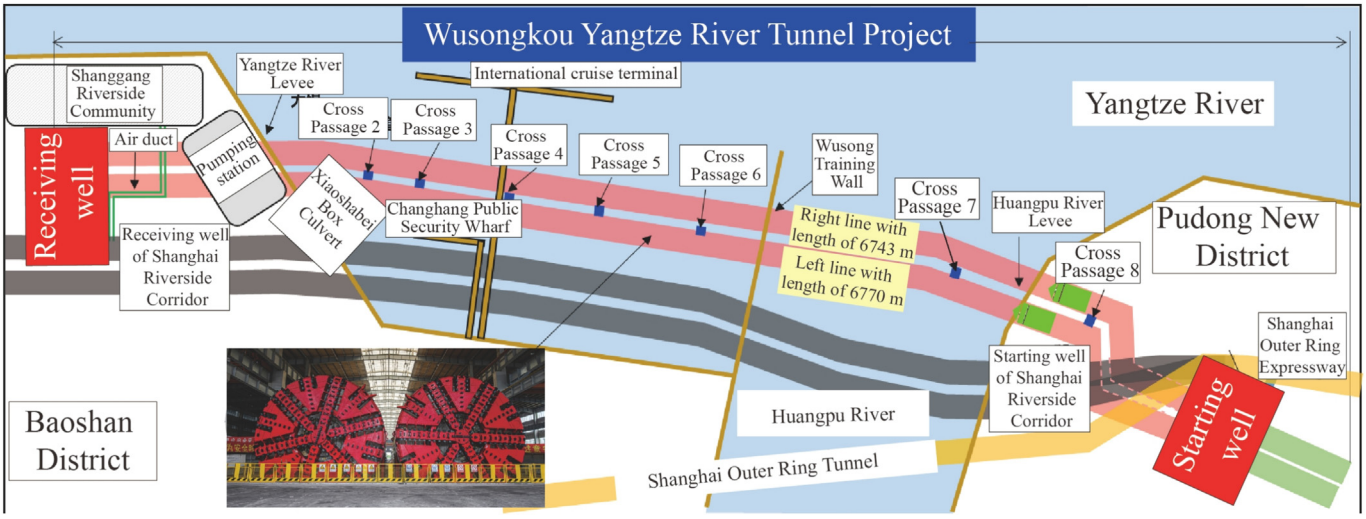

Fig. 25. Plan diagram of the engineering project.

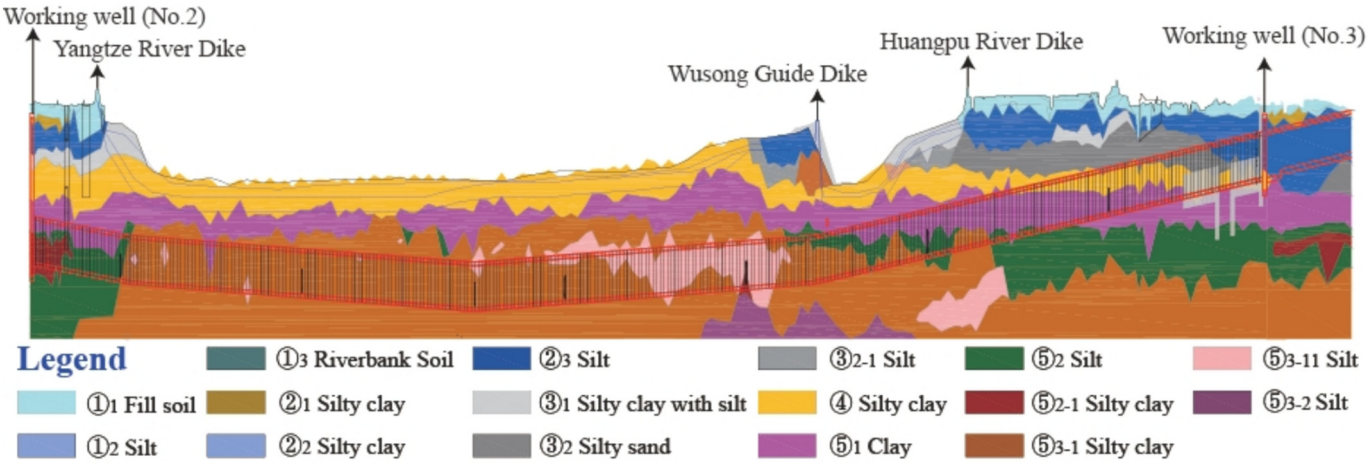

Fig. 26. Geological profile.

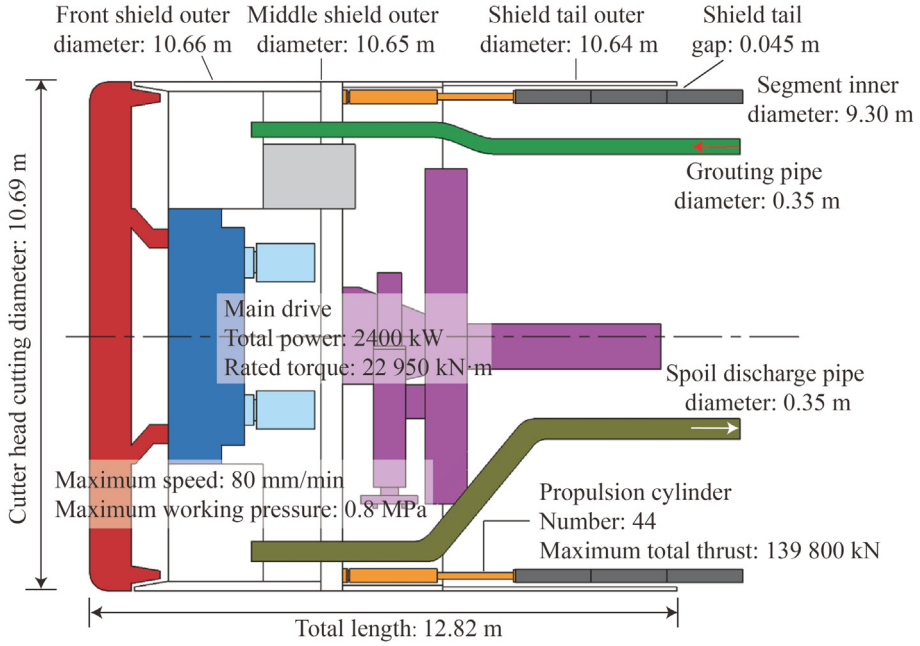

Fig. 27. Key parameters of the shield machine.

the longest distance driven by a large-diameter shield machine in soft strata within a single month, 868 m, was achieved in October 2023.

5.2 Analysis of application results

5.2.1 Thrust force and shield speed

Ten consecutive segmental rings, ranging from the 2969th ring to the 2978th ring, were selected as a representative case for data analysis and technical assessment of the system's application performance. Figure 28 presents the variations between the target and actual thrust forces for these ten rings. It is evident that the target total thrust generated by the thrust-vectoring automatic control system was slightly higher than the actual thrust values. This margin was intentionally designed to ensure the shield machine's stable advancement without reducing its speed during continuous excavation. Owing to the precise regulation of the oil pressure in each propulsion hydraulic cylinder, the actual thrust forces are closely aligned with the target values, with a deviation of approximately 2.5%. As shown in Fig. 28, minor manual adjustments were made to the shield speed. The actual speed responded promptly and effectively to these adjustments. Overall, the shield machine maintained a consistent operational speed of approximately 60 mm/min, with the deviation between the actual and target speeds controlled within a narrow range of –1 to +1 mm/min. This confirms the effectiveness

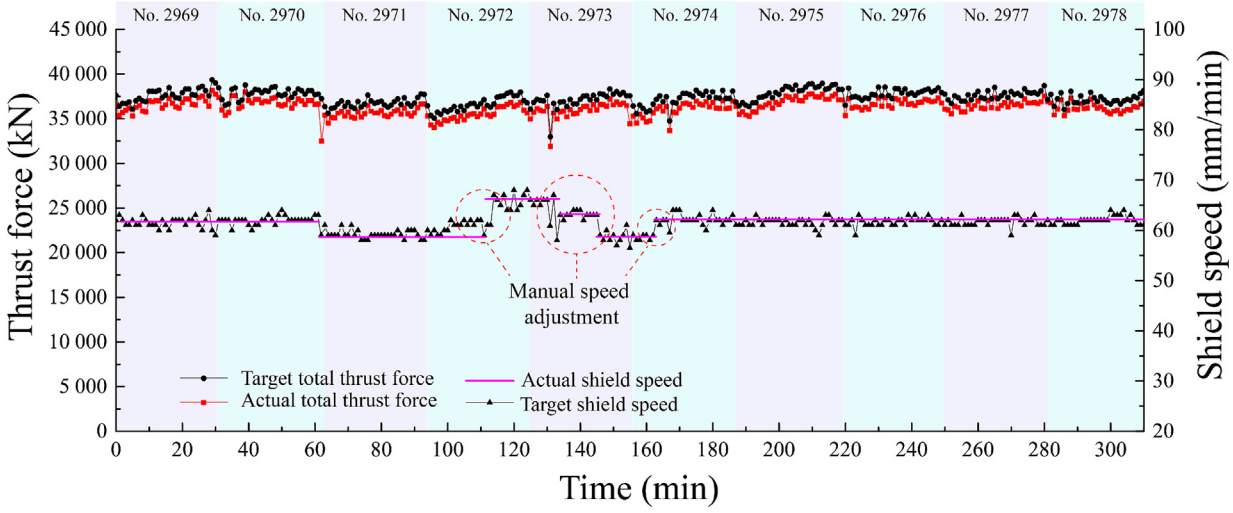

Fig. 28. Thrust force and shield speed.

of the thrust-vectoring automatic control system in regulating the shield speed, even in complex tunneling environments.

5.2.2 Thrust force moments

Figure 29 presents a comparison between the target and actual thrust force moments in both the horizontal and vertical directions. There is a high level of cooperativity between the target and actual moments in the two directions. However, throughout the entire process, the target values for both the horizontal and vertical moments were slightly greater than the actual values, maintaining a small deviation (approximately 10.0%) between the target and actual values. This approach was intended to ensure the thrust vector's ability to correct the shield attitudes.

In the actual shield tunneling process, the adjustment of the shield attitude is relatively sensitive and responsive due to the stable overburden depth and geological characteristics in the horizontal direction. However, in the vertical direction, the stability of the shield machine is relatively poor due to the direct influence of its own self-weight. Moreover, the physical properties of the geological layers may vary more significantly in the vertical direction, potentially resulting in greater load changes on the shield machine during the attitude adjustments, thereby increasing the control difficulty.

5.2.3 Shield attitudes

As illustrated in Fig. 30, the spatial interaction between the thrust action point and the shield attitudes in both the horizontal and vertical directions, as discussed in Section 2, displayed a cooperative relationship resembling the structure of "sugar-coated haws on a stick". Specifically, when the thrust action point moved in one direction, the shield attitude deviated in the opposite direction. Once the shield attitude reached the designated target values, the thrust action point shifted in the reverse direction to prevent over-correction. As a result, the overall trajectory of the shield attitude relative to the target values exhibited an "S-shaped" pattern, which aligns with the conventional operational experience in shield tunneling. The range of horizontal movement for the thrust action point was between –0.2 and 1.0 m, while in the vertical direction, it ranged from –1.0 to –0.4 m. Compared with the traditional manual control, the automation system significantly improved the stability of the shield machine.

There is a situation that requires explanation. When the shield tunneling reached rings 2969 and 2970, issues arose with ground spoil obstruction due to the extreme weather conditions. To avoid the clogging of the grouting pipeline, the construction team implemented a strategy of pausing the shield machine approximately every 0.2 m of advancement for about 2 h, until the ground spoil could flow freely. Consequently, the intelligent control system also experienced multiple start-stop cycles. During data processing, the data from the shield downtime phases were deleted, which resulted in an asymmetrical representation of the changes particularly in the vertical direction. However, it can be seen from Fig. 30 that the intelligent control system still played an effective role in adjusting the shield attitudes.

In general, all propulsion hydro-cylinders are locked to prevent the shield machine from retreating during the process of assembling segments into a ring. However, due to the partial loss of thrust force within the segment assembly area, both the thrust and its action point are subject to fluctuations. This instability can, in turn, result in a "kowtow" phenomenon in the shield cutterhead's vertical attitude, with maximum attitude variation even exceeding 15 mm, while the influence of this phenomenon is comparatively minimal in the horizontal direction. As illustrated in Fig. 30(b), the shield attitude tends to return to the target values during the tunneling of the subsequent ring, further demonstrating the effectiveness and reliability of the thrust-vectoring automatic shield tunneling technology. While

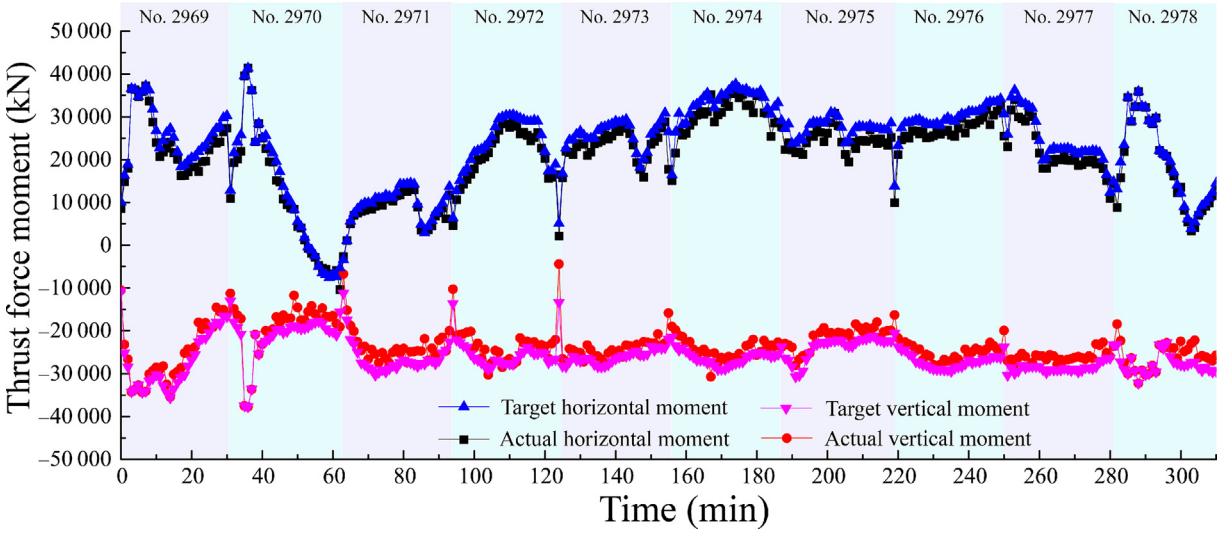

Fig. 29. Comparison between the target and actual moments of the thrust force.

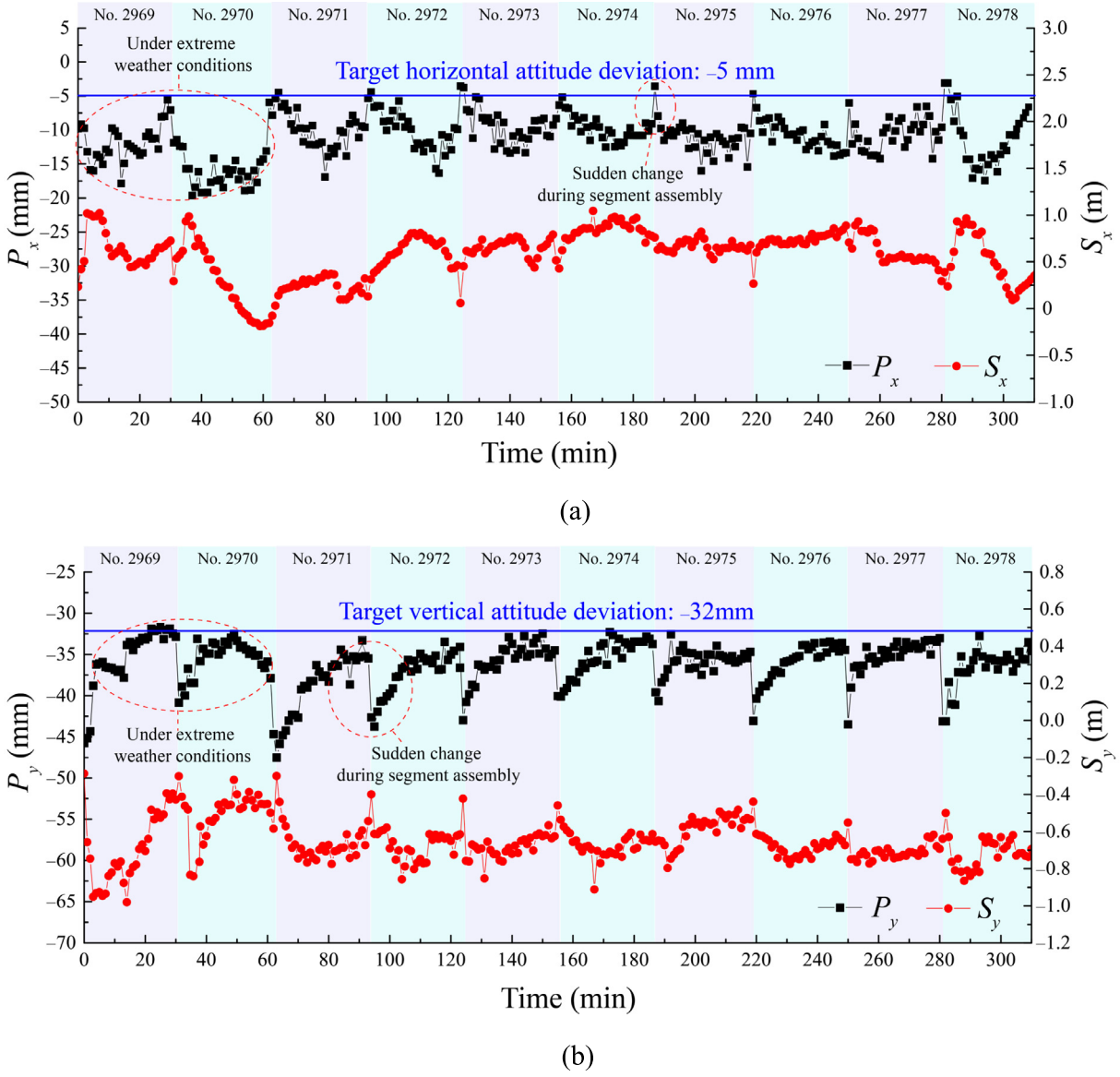

Fig. 30. Interaction between the shield attitudes and the moment of thrust force. (a) Horizontal direction, and (b) vertical direction.

additional factors, such as soil compression around the shield cutterhead and slight reductions in the support force acting on the tunnel face, also contribute to this phenomenon, the stabilization of the thrust vector remains a critical issue that warrants further investigation in future research.

To comprehensively elucidate the application stability of this thrust-vectoring automatic control system, this study presents the attitude deviation data of shield cutterhead for the segment rings ranging from the 2969th ring to 3068th ring, as depicted in Fig. 31. Despite the influence of abrupt attitude changes during the shield downtime, the overall control of the shield attitudes in the horizontal direction is maintained within the range of –20 to +5 mm. In comparison to the target value of –5 m, the control accuracy of the shield attitude is found to be from –15 to +5 mm. In the vertical direction, the shield attitudes are controlled within the range of –45 to –28 mm, relative to the target value of –32 mm, with control accuracy ranging from –13 to +4 mm. Drawing from construction experience, the control accuracy of shield attitudes under traditional manual control of large-diameter shield machines is ±30 mm in the horizontal direction and ±50 mm in the vertical direction. Comparative analysis reveals that this thrust-vectoring automatic shield tunneling technology significantly enhances the shield attitude control quality, thereby demonstrating its controllability and reliability.

The control accuracy of key parameters characterizes the level of automation control for this technology. Therefore, we have listed the control accuracy of key parameters that reflect the advantages of this technology, including shield thrust and its moments, shield speed, and shield attitudes, as shown in Table 1.

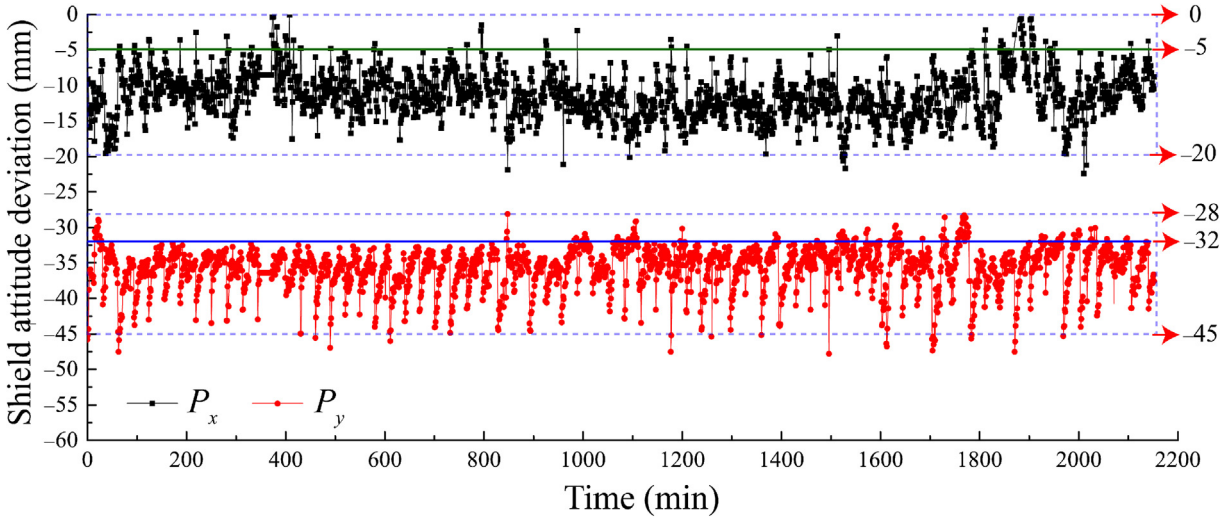

Fig. 31. Variations in shield attitudes over 100 consecutive segment rings.

Table 1
Control accuracy of the intelligent control system.

No.	Object	Range
1	Control accuracy of thrust force	2.5%
2	Control accuracy of thrust moments	10.0%
3	Control accuracy of shield speed	–1 to +1 mm/min
4	Shield attitude in horizontal direction	–20 to +5 mm
5	Shield attitude in vertical direction	–45 to –28 mm
6	Accuracy of attitude control considering the "kowtow" phenomenon in horizontal direction	–15 to +5 mm
7	Accuracy of attitude control considering the "kowtow" phenomenon in vertical direction	–13 to +4 mm

6 Conclusions

In this study, a thrust-vectoring automatic shield tunneling technology for shield machines was innovatively proposed based on an in-depth analysis of the motion control mechanisms governing shield tunneling operations. This technology integrates a control law for regulating shield attitude and speed, a motion path planning and navigation framework, and an automatic thrust vector control method. The proposed system was validated through comprehensive full-scale model tests and real-world engineering applications. The main contributions of this research are summarized as follows.

(1) Based on the defined shield thrust vector, a novel load-thrust "dual vector" motion control mechanism was introduced, and the moment vector generated by the interaction of the load and thrust vectors determines the yaw direction and yaw capability of the shield machine. Through data analysis from engineering projects conducted in soft, composite, and rock strata, a dynamic interaction between the shield attitude and the thrust action point was observed. This interaction was verified across varying geological conditions, demonstrating its robustness.

(2) A control law governing the thrust-vectoring automatic control system of shield machines was formulated using a parallel PID control system. This control law quantifies the relationship between variations in shield attitude and the displacement of the thrust action point. The feasibility and effectiveness of this control approach were preliminarily validated through full-scale model tests.

(3) Building upon the manual driving experience of shield tunneling machines, the motion path design and the generation of steering angles for each segmented advance distance were implemented following the introduction of the concept of CTA. An automatic control method for the thrust vector was developed, integrating feedforward calculation with feedback adjustment, driven by a fusion of mechanical principles and data analytics. This method was thoroughly validated through practical application in a large-diameter shield tunneling project, where it contributed to the achievement of a world record for monthly shield tunneling advance.

(4) Due to the high degree of coordination and consistency between the target and actual thrust vectors, stable shield machine operation was maintained under the control of the thrust-vectoring automatic

control system. A deviation of approximately 2.5% between the target and actual thrust forces was sustained, ensuring uniform-speed advancement. Furthermore, the target moments of the thrust force were deliberately set slightly higher than the actual values to enhance the shield machine's attitude adjustment capability. A key interactive feature, resembling the "sugar-coated haws on a stick" pattern, was identified, which confirmed the precise control relationship between the total thrust action points and the shield attitude deviation points.

Although the effectiveness and efficiency of the proposed method has been verified by both in-door laboratory tests and one engineering project, several important research topics remain to be explored, including the application of thrust-vectoring technology in composite and rock strata to assess its generalizability, the development of thrust vector maintenance methods during segment assembly to address the "kowtow" phenomenon, and the implementation and application of this technology on existing shield machines to evaluate its portability. These issues are currently being addressed.

It is also important to note that the classic PID control law was solely employed for system debugging purposes to assess the functionality of the intelligent control system, the computation and execution of target pressure for the thrust cylinders, and the responsiveness of the shield attitudes. However, due to safety concerns in engineering applications arising from the non-uniform nature of actual geological strata, the classic PID control was not deployed in practice.

Furthermore, although the control principles for thrust-vectoring in the propulsion systems are consistent across different types of shield machines, the application of this technology will not be limited by the type of shield machine. Currently, we have completed minor modifications on two existing traditional metro shield machines (earth pressure balance shield with a diameter of 6.76 m and equipped with a four-zone propulsion system) to enable automatic tunneling capabilities. These two modified machines have successfully completed the excavation of the section tunnel between Linghe Road Station and Yanggao North Road Station on Shanghai Metro Line 21 (with a total length of approximately 1900 m for both the up and down lines). Moreover, the interaction between the shield and the surrounding rock-soil mixture varies with different geological formations. For instance, when tunneling through composite strata, the interaction differs from that in soft soils, primarily reflected in the tuning results of the core parameters for shield attitude control law. Now, we are currently developing a 12 m diameter slurry balance shield, which is expected to be applied in an engineering project in Macao by June 2025. Considering that the ridge regression algorithm can achieve stable and compatible results either using time or distance as a variable in Eqs. (17) and (18), without involving issues of algorithm convergence, the determination of feedback duration or distance will be further evaluated according to the geological conditions, aiming to enhance the adaptability of this new technology in composite strata.

Data availability

The data that support the findings of this study are available from the corresponding author upon reasonable request.

CRediT authorship contribution statement

Yeting Zhu: Writing – original draft, Methodology, Formal analysis. **Di Wu:** Data curation. **Zhihua Wang:** Investigation. **Zixin Zhang:** Conceptualization, Supervision. **Shuaifeng Wang:** Visualization, Software. **Xin Huang:** Writing – review & editing, Validation, Supervision. **Yuan Qin:** Validation. **Yanfei Zhu:** Project administration, Funding acquisition. **Fan Wang:** Resources.

Declaration of competing interest

The authors declare that they have no known competing financial interests or personal relationships that could have appeared to influence the work reported in this paper.

Acknowledgement

The research was supported by the State-owned Assets Supervision and Administration Commission of Shanghai, China (Grant No. 2022020).

References

Afridi, S., Khan, T. A., Shah, S. I. A., Shams, T. A., Mohiuddin, K., & Kukulka, D. J. (2023). Techniques of fluidic thrust vectoring in jet engine nozzles: A review. *Energies, 16*(15), 5721.

Cai, J. (2022). Research and application of shield automatic tunneling technology based on multilayer perceptron autoregressive model. *Tunnel Construction, 42*(10), 1797–1803 (in Chinese).

Festa, D., Broere, W., & Bosch, J. W. (2015). Kinematic behaviour of a tunnel boring machine in soft soil: Theory and observations. *Tunnelling and Underground Space Technology, 49*, 208–217.

Fu, X. L., Ponnarasu, S., Zhang, L. M., & Tiong, R. L. K. (2024). Online multi-objective optimization for real-time TBM attitude control with spatio-temporal deep learning model. *Automation in Construction, 158*, 105220.

Fu, X. L., Wu, M. Z., Ponnarasu, S., & Zhang, L. M. (2023). A hybrid deep learning approach for dynamic attitude and position prediction in tunnel construction considering spatio-temporal patterns. *Expert Systems with Applications, 212*, 118721.

He, B. N., Zhu, G. L., Han, L., & Zhang, D. L. (2020). Adaptive-neuro-fuzzy-based information fusion for the attitude prediction of TBMs. *Sensors, 21*(1), 61.

Hu, M., Wu, B. J., Zhou, W. B., Wu, H. M., Li, G., Lu, J., Yu, G., & Qin, Y. (2022). Self-driving shield: Intelligent systems, methodologies, and practice. *Automation in Construction, 139*, 104326.

Huai, R. G., Huang, S. Y., Zhong, X. C., Chen, X. Q., & Hu, Y. K. (2022). Development and engineering application of novel synchronous double component grouting behind shield segment. *Tunnel Construction, 42*(9), 1521–1528 (in Chinese).

Invernizzi, D., & Lovera, M. (2018). Trajectory tracking control of thrust-vectoring UAVs. *Automatica, 95*, 180–186.

Invernizzi, D., Lovera, M., & Zaccarian, L. (2020). Dynamic attitude planning for trajectory tracking in thrust-vectoring UAVs. *IEEE Transactions on Automatic Control, 65*(1), 453–460.

Jia, G. P., Huo, J. Z., Yang, B. W., & Wu, Z. (2023). The real-time optimal attitude control of tunnel boring machine based on reinforcement learning. *Applied Science, 13*(18), 10026.

Jian, P., Yang, C., You, Y. S., Jin, L. J., Zang, J. Q., & Xu, S. T. (2023). Research and application of automatic control technology for shield tunneling attitude. *Tunnel Construction, 43*(10), 1795–1800 (in Chinese).

Kong, X. X., Ling, X. Z., Tang, L., Tang, W. C., & Zhang, Y. F. (2022). Random forest-based predictors for driving forces of earth pressure balance (EPB) shield tunnel boring machine (TBM). *Tunnelling and Underground Space Technology, 122*, 104373.

Li, L., Hu, C. M., & Hou, Y. J. (2020). Prediction analysis of shield vertical attitude based on GRU. *Journal of Physics: Conference Series, 1651*(1), 012032.

Li, X. F., & Gong, G. F. (2019). Predictive control of slurry pressure balance in shield tunneling using diagonal recurrent neural network and evolved particle swarm optimization. *Automation in Construction, 107*, 102928.

Liu, T., Gong, G. F., Yang, H. Y., Chen, Y. X., & Zhu, Y. (2019). Trajectory control of tunnel boring machine based on adaptive rectification trajectory planning and multi-cylinders coordinated control. *International Journal of Precision Engineering and Manufacturing, 20*, 1721–1733.

Qian, Q. H., Hu, X. Q., Li, S. C., Chen, J., & Zhu, W. B. (2024). Recent advances in key technologies of shield tunnel engineering in China. *Tunnel Construction, 44*(5), 897–926 (in Chinese).

Ren, Y. Y., Sun, Z. C., & Chu, C. H. (2019). An attitude control strategy for shield thrusting. *Tunnel Construction, 39*(6), 1038–1044 (in Chinese).

Soranzo, E., Guardiani, C., & Wu, W. (2023). Reinforcement learning for the face support pressure of tunnel boring machines. *Geosciences, 13*(3), 82.

Sun, W., Shi, M. L., Zhang, C., Zhao, J. H., & Song, X. G. (2018). Dynamic load prediction of tunnel boring machine (TBM) based on heterogeneous in-situ data. *Automation in Construction, 92*, 23–34.

Tang, L., Kong, X. X., Ling, X. Z., Zhao, Y. Z., Tang, W. C., & Zhang, Y. F. (2022). Deviation correction strategy for the earth pressure balance shield based on shield-soil interactions. *Frontiers of Mechanical Engineering, 17*, 20.

Tian, H. M., & Wang, Y. (2023). Data-driven and physics-informed Bayesian learning of spatiotemporally varying consolidation settlement from sparse site investigation and settlement monitoring data. *Computers and Geotechnics, 157*, 105328.

Wang, K. Y., Wu, X. G., Zhang, L. M., & Song, X. Q. (2023a). Data-driven multi-step robust prediction of TBM attitude using a hybrid deep learning approach. *Advanced Engineering Informatics, 55*, 101854.

Wang, L. T., Yang, X., Gong, G. F., & Du, J. N. (2018). Pose and trajectory control of shield tunneling machine in complicated stratum. *Automation in Construction, 93*, 192–199.

Wang, L. T., Zhu, F. Z., Li, J., & Sun, W. (2023b). A data-driven approach for modeling and predicting the thrust force of a tunnel boring machine. *Journal of Zhejiang University- SCIENCE A, 24*, 801–816.

Wang, P., Kong, X. G., Guo, Z. K., & Hu, L. (2019). Prediction of axis attitude deviation and deviation correction method based on data driven during shield tunneling. *IEEE Access, 7*, 163487–163501.

Wang, X. Y., Wang, X. Y., Ma, B., Li, Q., Wang, C. P., & Shi, Y. Q. (2023c). High-performance reversible data hiding based on ridge regression prediction algorithm. *Signal Processing, 204*, 108818.

Wang, X. Y., Yuan, D. J., Jin, D. L., Jin, H., Yang, Y., & Wu, J. (2022). Determination of thrusts for different cylinder groups during shield tunneling. *Tunnelling and Underground Space Technology, 127*, 104579.

Xie, P., Chen, K., Yin, Z. W., Zhu, Y. T., Luo, H. B., & Zhang, Q. B. (2024). A BIM-based multi-model framework for advancing TBM performance part 1: Real-time prediction of thrust force. *Tunnelling and Underground Space Technology, 151*, 105856.

Xu, J., Bu, J. F., Qin, N., & Huang, D. Q. (2024). SCA-MADRL: Multiagent deep reinforcement learning framework based on state classification and assignment for intelligent shield attitude control. *Expert Systems with Applications, 235*, 121258.

Yue, M., Sun, W., & Hu, P. (2012). Dynamic coordinated control of attitude correction for the shield tunneling based on load observer. *Automation in Construction, 24*, 24–29.

Zeng, L., Shu, W. Q., Liu, Z., Zou, X. Y., Wang, S. S., Xia, J. Y., Xu, C., Xiong, D. D., & Yang, Z. (2022). Vision-based high-precision intelligent monitoring for shield tail clearance. *Automation in Construction, 134*, 104088.

Zhang, N., Zhang, N., Zheng, Q., & Xu, Y. S. (2022a). Real-time prediction of shield moving trajectory during tunnelling using GRU deep neural network. *Acta Geotechnica, 17*, 1167–1182.

Zhang, Q., Qu, C. Y., Cai, Z. X., Kang, Y. L., & Huang, T. (2014). Modeling of the thrust and torque acting on shield machines during tunneling. *Automation in Construction, 40*, 60–67.

Zhang, W. J., Yang, Y., Zhang, C., Zhang, G. L., He, L. C., & Lu, J. R. (2023a). Dynamic autonomous deviation correction of super-large diameter shield tunnel rings based on multi-objective control techniques. *China Journal of Highway and Transport, 36*(11), 231–243 (in Chinese).

Zhang, W. S., Liu, X. Y., Zhang, L. Y., & Wang, Y. D. (2023b). Intelligent real-time prediction of multi-region thrust of EPB shield machine based on SSA-LSTM. *Engineering Research Express, 5*(3), 035013.

Zhang, Y. K., Gong, G. F., Yang, H. Y., Chen, Y. X., & Chen, G. L. (2022b). Towards autonomous and optimal excavation of shield machine a deep reinforcement learning-based approach. *Journal of Zhejiang University-SCIENCE A, 23*(6), 458–478.

Zhen, M., Dong, X. Z., Liu, X. Y., & Tan, C. Q. (2024). Accelerated formulation of optimal control law for adaptive cycle engines: A novel design methodology. *Aerospace Science and Technology, 148*, 109076.

Zheng, Z., Luo, K. D., Tan, X. Z., Jia, L. H., Xie, M. R., Xie, H. B., Jiang, L. J., Gong, G. F., Yang, H. Y., & Han, D. (2024). Autonomous steering control for tunnel boring machines. *Automation in Construction, 159*, 105259.

Zhou, B., & Zhao, M. (2020). Numerical simulation of thruster-thruster interaction for ROV with vector layout propulsion system. *Ocean Engineering, 210*, 107542.

Zhu, Y. T., Zhu, Y. F., Chen, E. J., Zhai, Y. X., Min, R., Tang, B., & Huang, X. (2023). Synchronous shield tunnelling technology combining advancement and segment fabrication: Principle, verification and application. *Underground Space, 13*, 23–47.